Arabian Journal of Chemistry (2023) **16**, 104471

King Saud University

Arabian Journal of Chemistry

www.ksu.edu.sa
www.sciencedirect.com

ORIGINAL ARTICLE

Enhancement of Cd^{2+} removal on CuMgAl-layered double hydroxide/montmorillonite nanocomposite: Kinetic, isotherm, and thermodynamic studies

Fatin A. Alnasrawi [a,*], **Ahmed A. Mohammed** [b]

[a] *Department of Civil Engineering, College of Engineering, Kerbala University, Karbala, Iraq*
[b] *Department of Environmental Engineering, College of Engineering, University of Baghdad, Iraq*

Received 25 September 2022; accepted 26 November 2022
Available online 5 December 2022

KEYWORDS

Adsorption;
Cd^{2+};
CuMgAl-LDH;
Montmorillonite;
Nanocomposite;
Regeneration

Abstract In recent decades, great progress has been made in the application of adsorption processes to mitigate water pollution by hazardous metals. However, developing a highly efficient adsorbent is essential if the adsorption process is to be successfully applied in practical applications. In this study, a CuMgAl-layered double hydroxides/montmorillonite nanocomposite (CuMgAl-LDH/MMt) was prepared, characterized, and then used as a novel adsorbent for adsorption of Cd^{2+} ions from wastewater. The effects of initial pH, adsorbent dosage, agitation speed, particle size, contact time, initial Cd^{2+} concentration, and temperature on the pollutant removal efficiency were analyzed. An isotherm model reading revealed that the results of the experimental work were a good fit with the Freundlich model. The maximum adsorption capacity was reached at 174.87 mg/g under optimal conditions (pH 5, dosage of 0.02 g/l, agitation speed of 150 rpm, and particle size of 87 μm) at 50 ppm after 120 min of adsorption time. Kinetic studies showed that pseudo-second-order models were best fitted to the adsorption data, indicating heterogeneous adsorption of Cd^{2+} ions onto multilayer CuMgAl-LDH/MMt sites, and that the adsorption process is primarily chemical adsorption. Thermodynamic parameters (ΔS^o, ΔH^o, and ΔG^o) demonstrated that Cd^{2+} adsorption onto adsorbent was exothermic and spontaneous. Moreover, the synthesized adsorbent can be recovered after five consecutive cycles with a minimal reduction in the adsorption ability of 29.56 %. The study showed that specific heavy metals can be removed from aqueous solution by a newly prepared adsorbent due to its excellent morphology, high stability under a wide range of conditions, recyclability, and high adsorption capacity.

* Corresponding author.
E-mail address: fatinen35@gmail.com (F.A. Alnasrawi).

Peer review under responsibility of King Saud University.

Production and hosting by Elsevier

https://doi.org/10.1016/j.arabjc.2022.104471

Nomenclature

A_t	Temkin isotherm constant. (l/g)
b_T	Temkin constant related to heat of sorption, (J/mol)
C	Constant of intra particle diffusion, (mg/g)
C_0	Liquid-phase initial concentration, (mg/l)
C_e	Liquid-phase equilibrium concentration, (mg/l)
E	Adsorption energy, (kJ/mol)
ΔG^o	Gibbs free energy change, (kJ/mol)
ΔH^o	Standard enthalpy change, (kJ/mol)
K_d	Distribution coefficient, (ml/g)
K_{DR}	A constant of Dubinin-Radushkevich, $(mol/J)^2$
K_f	A constant of the Freundlich isotherm, $(mg/g)(l/mg)^{1/n}$
K_{id}	The constant of intra-particle diffusion, $(mg/g.min^{(1/2)})$
K_L	A constant of the Langmuir isotherm, (l/mg)
K_T	The equilibrium constant, (l/mg)
k_1	constant of pseudo first sorption, (1/min)
k_2	constant of pseudo second sorption, (g/mg.min)
n	Freundlich constant related to adsorption intensity
1/n	Heterogeneity factor
pzc	The point zero charge
q_e	Solute uptake (mg/g)
$q_{e,cal}$	Experimental solute uptake at equilibrium (mg/g)
$q_{e,exp}$	The calculated solute uptake mg/g)
q_{max}	A maximum solute uptake (mg/g)
R	Removal efficiency
R	The universal gas constant (8.314 J/mol K)
R^2	Coefficient of determination
R_L	Langmuir or equilibrium parameter
ΔS^o	Standard entropy change, (KJ/mol.K)
t	Time (min)
T	Temperature (K)
V	Volume of solution (l)
W	Adsorbent mass used (m)

Greek letters

ε	Dubinin-Radushkevich constan
δ	initial rate of adsorption
α	Initial rate of adsorption, (mg/g.min)

1. Introduction

The discharge of wastewater loaded with hazardous heavy metals into water bodies and natural ecosystems is a serious threat to human and environmental health (Mohammed et al., 2018; Wang et al., 2012). Heavy metals are not biodegradable and their high density and atomic weight make them environmentally stable (Peighambardoust et al., 2021). Cadmium, is a relatively rare metallic element, which a highly toxic metal that has caused serious threats to the environment and human health. Cd^{2+} can persist in the human body, as well as the bodies of other living organisms, for an extremely long time, and can cause lung damage, hypertension, hepatitis, bone damage, and muscle cramps (Foroutan et al., 2020b). One of the most significant environmental sources of cadmium is industrial discharge (Dubey et al., 2017). WHO sets the allowable limit for Cd^{2+} ions in drinking water at < 1 μg/L (Dang et al., 2020). Therefore the elimination of heavy metals from aquatic media is now one of the most challenging environmental issues (Nguyen et al., 2021). Many techniques have recently been proposed for removing cadmium from wastewater. These include, emulsion liquids (Mortaheb et al., 2009), ion-exchange (Wong et al., 2013), chemical coagulation and precipitation (Charerntanyarak, 1999), electrochemical techniques (Najwa et al., 2020), and adsorption (Mohammed, 2015). However, barring the last method(except that related to, the other techniques mentioned imply a few limitations that limit their widespread use. For example, they may generate secondary pollutants, have high operating costs, or be ineffective at low pollutant concentrations (Mohammed et al., 2018). The adsorption process has been intensively studied because of its ability to overcome all the disadvantages of conventional treatment techniques. This is due to its simplicity, cost effective technique, High metal binding capacities, adsorbent recyclability, and does not produce any toxic by-product (Dang et al., 2020; Yang et al., 2015). In the adsorption process, the capacity of the used adsorbents is the key factor in the fast and efficient adsorption of target pollutants. Thus, substances with a high surface area, and a large number of bending sites, make good adsorbents. Research has discovered many excellent adsorbents, both theoretical and practice one of the most effective being the layered double hydroxide [LDH]. Their use as adsorbents in water treatment has received great attention due to their large surface area and highly tunable interior architecture (Gu zi, 2015; Zubair et al., 2017), exchangeable anionic features (Zubair et al., 2017), and non-toxicity (Hoyo, 2007). LDHs therefore show a high adsorption capacity (Lu et al., 2016; Prasad et al., 2018). LDH, also known as hydrotalcite-like compounds, belong to a versatile class of bi-dimensional (2D) anionic lamellar nanostructured materials. The chemical composition of LDH is represented by the general formula:$[M^{++}{}_{1-x}.M^{+++}{}_x(OH)_2]^{+x}$ $\left[\left[(A^{-n})_{x/2}.m.H_2O\right]\right]^{-x}$ where M^{++} and M^{+++} represent the di- and tri-valent layer cations in octahedral positions within the hydroxide layers; A^{-n} is an anion and the charge density of the LDH layers, m is the number of water molecules occupying the interlamellar layer sites, where no anions are present (Daniel and Thomas, 2020). Additionally, the pure hydrotalcite phase can be obtained when × lies between 0.2 and 0.33, where × is the ratio $M^{+++}/(M^{++}+M^{+++})$(Bukhtiyarova, 2019; Cao et al., 2016; Daniel and Thomas, 2020). However, LDH could hardly adsorb a cationic ion due to ion repulsion from positive sheets, limiting its utility. Recently, LDH based nanocomposites such as those hybridized with carbon materials, anions, or polymers, have been intensively researched, as they have the ability to remove many types of hazardous material. The research has led to improvements in their surface area and anion exchange ability, and shown them to have excellent selectivity (Zubair et al., 2017). Montmorillonite (MMt) is a clay mineral consisting of an Al^{3+} octahedral adjoining two sheets of Si^{4+} tetrahedral. When Mg^{2+} or Zn^{2+} is substituted for Al^{3+}, a perpetual negative charge develops on the surface of the MMt and the interlayer. Various cations may hybridize into the MMt layers to neutralize the negative charge. Several findings demonstrate that MMt is excellent for the removal of dye (Ai et al., 2011; Almeida et al., 2009). In addition, previous studies have shown the combination of MMt and LDH to be an effective adsorbent for the removal of MO (Jiang et al., 2019a) and MB (Kute et al., 2018). To the best of our knowledge, there has been no work investigating the use of CuMgAl-LDH/MMt, synthesized by the co-precipitation method, for the adsorption of cadmium from aqueous solutions. This study had four aims: (i) to develop a new adsorbent composite of LDH and MMt for the removal of metal cations; (ii) to examine the physiochemical characteristics of synthe-

sized CuMgAl-LDH/MMt using transmission electron microscopy (TEM), powder X-ray diffraction patterns (XRD), Brunauer–Emmet t–Teller analysis (BET), field-emission scanning electron microscopy (SEM), energy dispersive X-ray spectroscopy (EDX), and Fourier transform infrared spectra (FTIR), to understand more about the adsorption mechanism; (iii) to evaluate the adsorption capacity for Cd^{2+} under different experimental conditions (initial pH, adsorbent dosage, agitation speed, particle size, contact time, initial Cd^{2+} concentration, and temperature); and (iv) to examine kinetic and isotherm adsorption models, as well as thermodynamic adsorption models.(See Scheme 1).

2. Materials and methods

2.1. Materials

Montmorillonite K 10 clay (cation exchange capacity (CEC) = 48 m_{eq}/100 g) was purchased from Nanosany Co., the chemical compositions of montmorillonite (wt%) are SiO_2 50.95 %, Al_2O_3 19.60 %, Fe_2O_3 5.62 %, MgO 3.29 %, CaO 1.97 %, Na_2O 0.98 %, K_2O 0.86 %, TiO_2 0.62 %, LOI 15.45 %. The chemicals used in this study copper nitrate trihydrate $Cu(NO_3)_2{\cdot}3H_2O$ (>95 %), magnesium nitrate hexahydrate $Mg(NO_3)_2{\cdot}6H_2O$ (>98 %), aluminum nitrate nonahydrate $Al(NO_3)_3{\cdot}9H_2O$ (>98 %), and cadmium nitrate tetrahydrate $Cd(NO_3)_2{\cdot}4H_2O$ (>98 %), also NaOH and HCL were used without further purification. The cadmium solutions were prepared using deionized water.

2.2. Synthesis of CuMgAl-LDH/MMt

The CuMgAl-LDH/MMt nanocomposite is considered a superior adsorbent for cationic ion removal. It was synthesized using the low-supersaturation co-precipitation method at constant pH giving a metal composition in the range ($0.25 < x < 0.33$). The cation salts of $Mg(NO_3)_2{\cdot}6H_2O$, $Cu(NO_3)_2{\cdot}3H_2O$, and $Al(NO_3)_3{\cdot}9H_2O$ had molar ratios (Cu^{2+}, Mg^{2+}: Al^{3+}) and (Cu^{2+}: Mg^{2+}) of 2:1 and 1:1 respectively, and were added to 40 ml deionized water, and the mixture stirred for 2 h at room temperature. 5 g of MMt was dispersed in 500 ml of water and heated at 50 °C for 30 min with vigorous agitation. The cation salts solution and MMt solution were simultaneously added dropwise to the 200 ml of deionized water and stirred for 3 h. The reaction pH was maintained at a constant value of 9 ± 0.1 by adding 1 M NaOH (sketch 1). The mixture was aged for 12 h at 100 °C then filtered, washed three-times with deionized water, and oven-dried at 65 °C for 12 h. The claybank has appeared, and the possible reaction can be described in the following Eq. (1).

$$Al^{3+} + Cu^{2+} + Mg^{2+} + NO_3^{2-} + OH^- \rightarrow CuMgAl - NO_3^{2-} LDH \quad (1)$$

MMt is used as a base for the direct growth of CuMgAl-LDH. The interaction between the Cu^{2+}, Mg^{2+}, and Al^{3+} and the OH^- leads to the formation of CuMgAl-LDH on the MMt, in which NO_3^{2-} ions are intercalated into the interlayer structure to balance the charge.

2.3. Characterization

Transmission electron microscopy was used to investigate the nanostructures of the synthesized CuMgAl-LDH/MMt (TEM, Philips, CM120). The crystallinity of the samples were described by Powder X-ray diffraction patterns (XRD), which were recorded by a Siemens-D500 diffractometer with CuK_α radiation, operating at 40 kV, 40 mA, and $\lambda_{CuK\alpha}$ = 1.5418 Å at a scan rate of 0.05° s^{-1} across a 2θ range of 0 – 80°. A Brunauer–Emmett–Teller analysis (BET) was used to determine specific surface areas and pore size distributions. Field-Emission Scanning Electron Microscopy (SEM, ZEISS, UK) outfitted with energy dispersive X-ray spectroscopy (EDX) was used to characterize the surface morphology and elemental distribution of the samples. Fourier transform infrared spectra in the range of 380–4000 cm^{-1} were used to describe the surface functional groups of the materials (FIIR, Jasco 4200, Japan). The point zero charge (pH pzc) of the CuMgAl-LDH/MMt adsorbents were identified by preparing a 40 ml solution of (0.1 M) $NaNO_3$ and adjusting the pH of the solution with 0.1 M NaOH and/or HCl to obtain pH values in the range 2–12. An amount of adsorbent was added to the solution which was then agitated at a speed of 150 rpm at a temperature

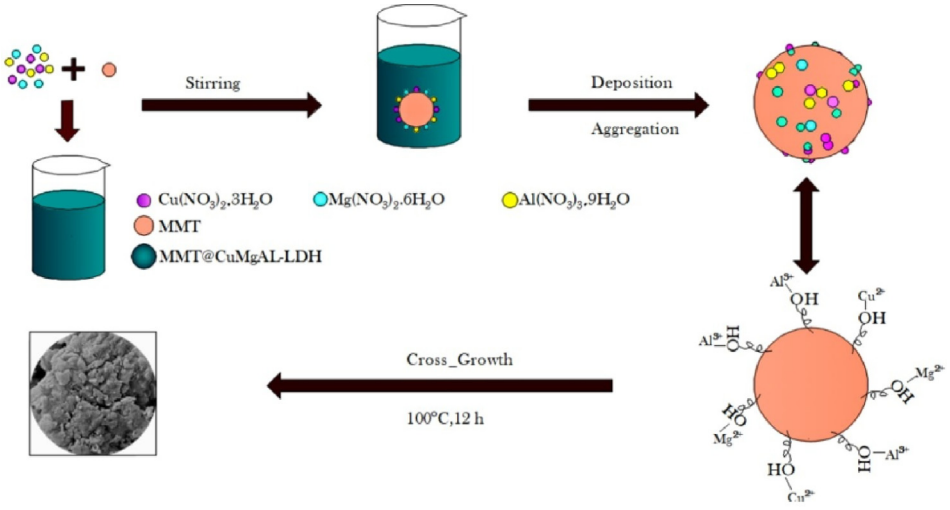

Scheme 1 Sectematic illustrate the cumgal-ldh/mmt.

of 30 °C for 24 h. The mixture was then filtered to separate the solid particles, and the final solution pH was tested. The pH_{PZC} of the CuMgAl-LDH/MMt adsorbent is the intersection point in the plot of final by (initial-final) pH (Begum et al., 2021; Mohammed and Kareem, 2019).

2.4. Batch experiments for Cd^{2+} removal

Batch adsorption experiments were carried out to determine the Cd^{2+} removal performance of the as-prepared adsorbent. The effects of pH (2–8), CuMgAl-LDH/MMt (0.05–0.3 gm/100 ml Cd^{2+} solution dosage, agitation speed (100–250 rpm), particle size (87, 122, 194 μm), and initial concentration of Cd^{2+} (20–70 ppm) on the removal of cadmium ions was studied. The Cd^{2+} uptake on the CuMgAl-LDH/MMt nanocomposite was evaluated as a function of time (5–180 min) to determine the time required to reach equilibrium. A kinetic adsorption process was employed to evaluate the equilibrium time of Cd^{2+} adsorption on LDH to examine its mechanism and rate-controlling step. This was done by combining 0.25 mg of LDH with 100 ml of Cd^{2+} solution in concentrations ranging from 20 mg/l to 70 mg/l at 298 K and an initial pH of 5, adjusted with 0.1 M HCL and 0.1 M NaOH. This process is primarily time-dependent.

To determine the effect of temperature, the experiments were performed under the optimal conditions determined by previous experiments, and the temperature was adjusted (25, 30, 35, 40 °C) using an incubator shaker.

In each experiment, a quantity of adsorbate (mg) was reacted with 100 ml of Cd^{2+} solution and shaken for 180 min. After adsorption, the mixture of CuMgAl-LDH/MMt and cadmium ions was separated using 0.45 μm filter paper. The residual metal ions in the solution were analyzed using an atomic absorption spectrophotometer (AAS) (AA-7000, Shimadzu Corporation, Japan). The removal efficiency, and adsorption amount of adsorbate for Cd^{2+}, were calculated by using equations (2) and (3), respectively.

$$\text{Removal efficiency}\,(\%) = \frac{C_0 - C_e}{C_0} * 100 \tag{2}$$

$$q_e = \frac{(C_0 - C_e)V}{m} \tag{3}$$

where q_e is the adsorption capacity; C_0 and C_e are the initial and equilibrium concentrations of Cd^{2+}, respectively; m is the mass of adsorbate, and V is the volume of solute.

2.5. Statistical analysis

To compute the isotherm and kinetic model parameters, trial and error nonlinear regression analysis was performed using the Solver add-in in Microsoft Excel. Eq. (4) was used to calculate the determination coefficients (R^2) of the nonlinear optimization models. To identify the best fitting adsorption model, chi-square values (X^2) were determined alongside non-linear R^2 (Tran et al., 2018).

$$R^2 = 1 - \frac{\sum (q_{e,exp.} - q_{e,cal.})^2}{\sum (q_{e,exp.} - q_{e,mean})^2} \tag{4}$$

$$X^2 = \sum \frac{(q_{e,exp.} - q_{e,cal.})^2}{q_{e,exp.}} \tag{5}$$

Where: $q_{e,exp}$ is experimental solute uptake at equilibrium (mg/g), $q_{e,cal}$ is the solute uptake calculated from the corresponding isotherm and kinetic model(mg/g), and $q_{e,mean}$ is the mean of $q_{e,exp}$ values (mg/g).

3. Results and discussions

3.1. Characterization of MMT, CuMgAl-LDH, CuMgAl-LDH/MMt

The morphology of the prepared nanoadsorbent's internal structure was investigated using transmission electron microscopy (TEM). The TEM micrographs in Fig. 1 demonstrate that the CuMgAl-LDH/MMt nanocomposites have irregular shapes, but the vast majority of them are roughly integrated spherical hierarchical particles with variable crystallite sizes. The LDH was well dispersed across the MMt substrate surface with minimal agglomeration, and it was neither too dense to

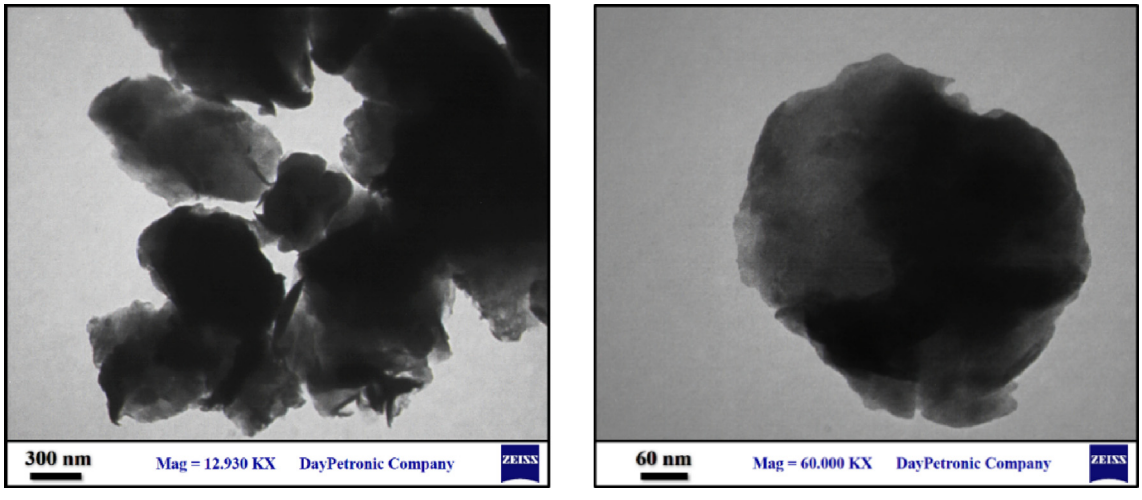

Fig. 1 TEM image of synthesized CuMgAl-LDH/MMt adsorbent.

block neighboring particles nor too sparse to provide enough active sites. LDH acts like monodispersed particles, rather than multidispersed particles, thus maximizing the surface area available for contaminant molecule adsorption (Mohammed and Kareem, 2019). The inclusion of a MMt substrate may significantly inhibit the LDHs aggregation due to the oxygen-containing functional groups on the MMt nanoparticles that provide nucleation sites for the growth of LDH (Yang et al., 2013). It can be concluded that by growing LDH on MMt, the ion exchange and surface adsorption abilities of LDH may be effective in removing heavy metal ions from liquid solutions.

The crystallinity of the LDHs was described by their Powder X-ray diffraction patterns (XRD). The XRD patterns of the substrate MMt, the precursor CuMgAl-LDH, and the prepared CuMgAl-LDH/MMt are shown in Fig. 2. The XRD pattern in Fig. 2a, of the (*00 l*) series diffraction peaks at (003), (006), and (009), are observed as narrow symmetric lines at low 2θ angles at 20.5, 31.6, and 41.5°, respectively, indicating a lamellar structure (Rathee et al., 2020).

The diffraction peaks of MMt in Fig. 2b, observed at 19.9, 26.6, 35.0, 39.6 and 45.9°, confirm the crystalline structure of MMt (Ahmadi et al., 2020) and are consistent with the standard pattern (JCPDS no. 03–0015), suggesting the presence of MMt in their structure. In addition, a peak related to the crystalline structure of (*00 l*) at 6.3° was seen in the MMt structure, indicating a layer structure in the MMt matrix (Foroutan et al., 2020a; Peighambardoust and Pourabbas, 2007).

The characteristic sharp peaks of CuMgAl-LDH/MMt at 2*θ* values of 12.4, 19.9, 20.9, 26.8, 27.8, 35.2, 36.7, 39.6, 50.3, 60.1, 62.1, and 68.3° (corresponding to the hydrotalcite lattice planes (*hkl*) planes of (100), (002), (200), (112), (210), (212), (220), (311), (411), (332), (324), and (504), respectively (JCPDS no. 012–0232)), were identified, and the interlayer spacing for CuMgAl-LDH/MMt calculated for these diffraction angles. The findings are shown in Fig. 2c. The well-defined diffraction peaks of CuMgAl-LDH/MMt can be indexed to a series of crystal planes, which is characteristic of hydrotalcite-like materials (Jiang et al., 2019b). and the narrow peaks are attributed to the high crystallinity of the prepared adsorbent (Rathee et al., 2020).

The diffraction peaks of (324) at high angles (near 2*θ* = 62.1°) reflect that the presence of three metal cations (Cu^{2+}, Mg^{2+} and Al^{3+}) in the host layer. The crystallite size for MMt, CuMgAl-LDH and CuMgAl-LDH/MMt was calculated using the Scherrer equation (Kareem and Mohammed, 2020) and found to be 2, 27.74, and 30.89 nm, respectively. This confirms the loading of MMt and the successful fabrication of particles in nano dimensions with a crystallinity order of 44.64 %.

As illustrated in Fig. 3, N2 sorption–desorption isotherms at 77 K were used to investigate the main textural (microstructural) properties of the substrate MMt, the precursor CuMgAl-LDH, and the as-synthesized CuMgAl-LDH/MMt adsorbent. The specific surface area was estimated by applying the BET equation with the total pore volume taken at P/Po = 1, and the pore size distribution was estimated by the BJH method. Based on the IUPAC classification, all tested samples were classified as IV-type isotherms and have a H3 type hysteresis loop (which extends down to P/Po = 0.42). It indicates that all adsorbents have the characteristic structure of mesopores (Santamaría et al., 2020) with average pore diameters of 6.83, 19.813, and 26.238, for the MMt-, LDH,

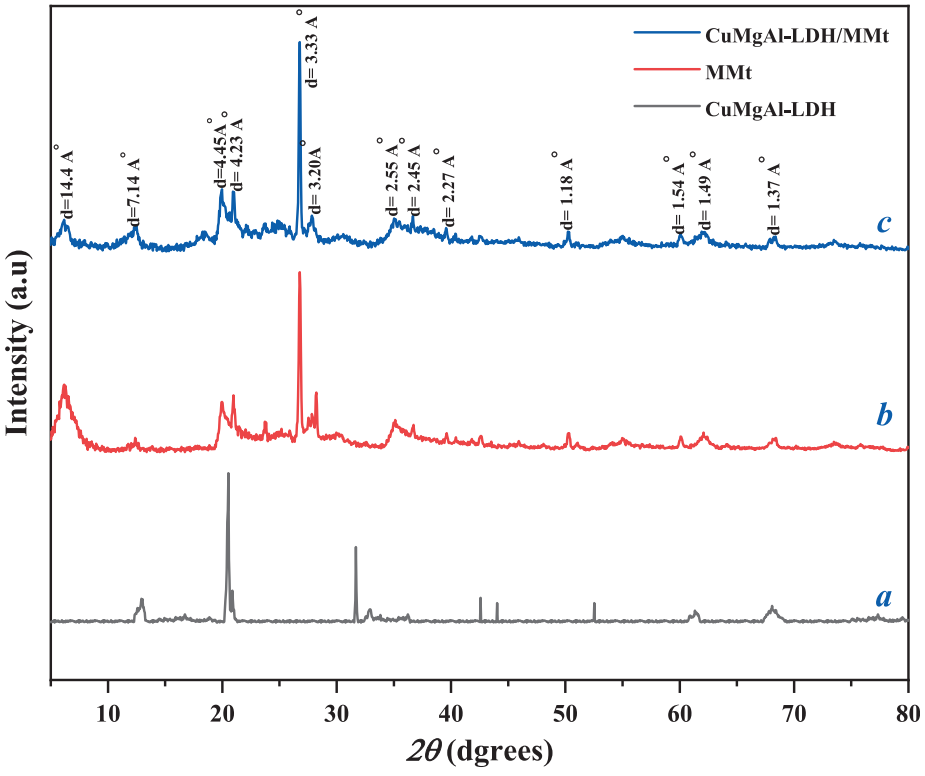

Fig. 2 XRD characterization of (a) CuMgAl-LDH, (b) MMt, (c) CuMgAl-LDH/MMt.

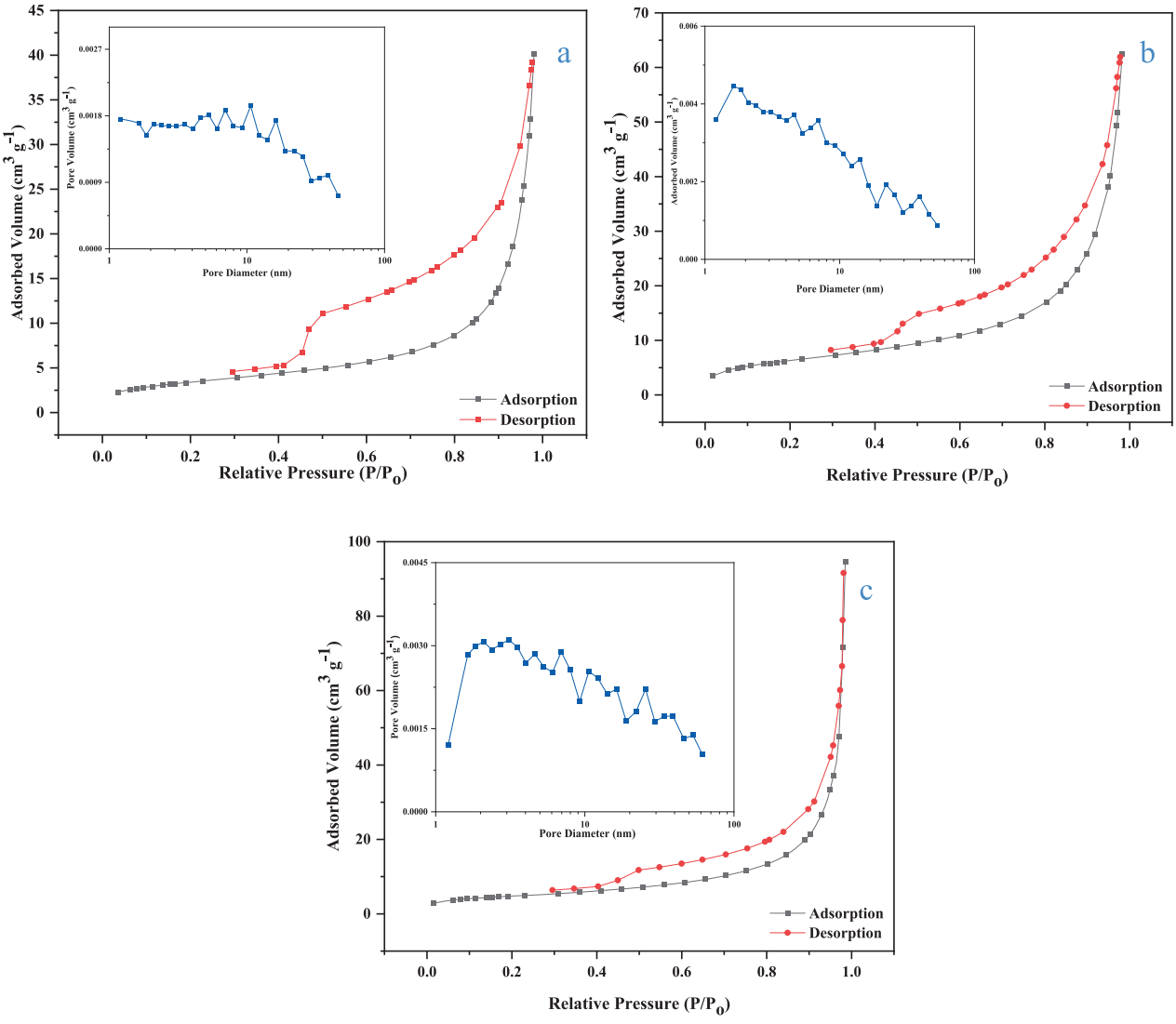

Fig. 3 N_2 adsorption/desorption isotherms and pore-size distribution of (a) MMt, (b) CuMgAl-LDH (c) CuMgAl-LDH/MMt.

and as-synthesized LDH-MMt hybrid, respectively. The extensive hysteresis loop demonstrates the successful fabrication of a mesoporous structure that permits the fast diffusion of inorganic pollutants during the adsorption process. This accelerates the reaction rate and provides a more active site for adsorption (Ahmed et al., 2017).

The BET surface areas of MMt and LDH as listed in Table 1 are 17.23 and 12.545 m^2/g, respectively, while that of the CuMgAl-LDH/MMt hybrid is higher at 77.62 m^2/g with a BET constant of 94.022. This indicates that precipitation of LDH into the MMt increased its specific surface area and improved its porosity, thus resulting in a comparatively greater uptake of Cd^{2+} ions (Foroutan et al., 2021a). This could be due to decreased agglomeration from the mixing of the two counterparts and preparation of the hybrid nano-filler (Mallakpour and Naghdi, 2020). As the BET results showed, a CuMgAl-LDH/MMt would has higher catalytic and adsorption activity also play an important role in the Cd^{2+} adsorption mechanism(Chen et al., 2012) than for MMt and LDH alone.

Table 1 The textural properties of MMt, LDH, and LDH/MMt.

Samples	BET Surface Area	Pore Volume	Average Pore Diameter
	(m^2/g)	(cm^3/g)	(nm)
MMt	12.5	0.062	19.8
CuMgAl-LDH	23.9	0.103	17.2
CuMgAl-LDH/MMt	77.6	0.156	26.2

Fig. 4a depicts the surface morphology of native MMt prior to the nonabsorbent preparation. This figure shows an irregular sphere-shaped possessing lamellar aggregates. Several minute cavities and pores can be seen suggesting that the surface of MMt facilitates the precipitation of metal salts during the synthesis of the nanocomposite. Fig. 4b shows the porous structure of CuMgAl-LDH/MMt. It can be clearly seen that layered materials grow directly on the surface of the spherical

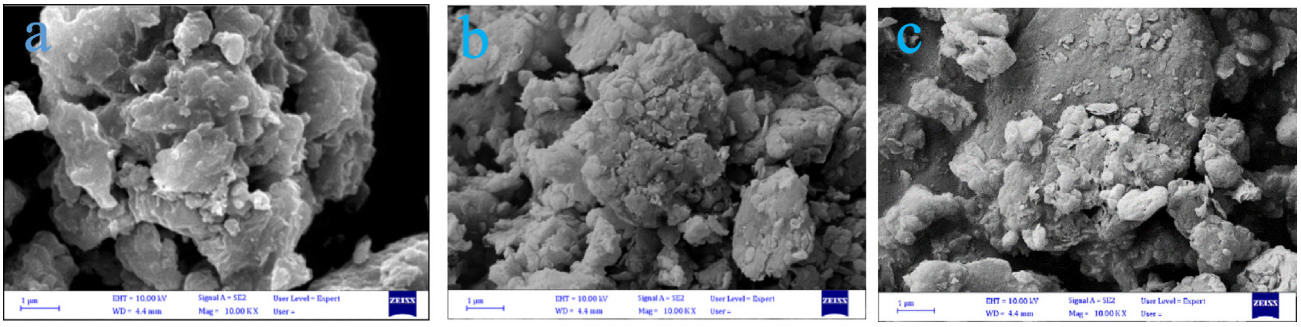

Fig. 4 SEM image of (a) MMt, (b) CuMgAl-LDH/MMt before adsorption, (c) CuMgAl-LDH/MMt after Cd^{2+} sorption.

MMt, and chemical bonding ensures a strong adhesion of CuMgAl-LDH to MMt. The results above indicate that the CuMgAl-LDHs film successfully modified the MMt. The layered structure embedded cavities of sizes ranging from 1.2 to 61.3 nm (as defined in N_2 sorption–desorption isotherms) that were scattered across the complete sample matrix. These cavities are large enough to enable heavy metal ions to penetrate the LDH structure where they are then able to interact with the surface groups. The morphology of CuMgAl-LDH/MMt was also observed using SEM after the sorption of Cd^{2+} ions (Fig. 4c). This figure suggests that the sorption of cadmium ions did not substantially alter the surface morphological characteristics of CuMgAl-LDH/MMt adsorbents. These results confirm that the CuMgAl-LDH/MMt has considerable stability in acidic environments(Ahmed et al., 2017). Furthermore, in all experiments the primary mechanism for cadmium removal by the synthesized LDHs was by ion exchange (Ma et al., 2014).

Energy dispersive spectrum (EDS) maps were taken on the SEM. The EDS mapping image in Fig. 5a shows the surface elements of MMt, whereas in Fig. 5b shows that the CuMgAl-LDH/MMt surface has elements of O, Si, Al, Mg, and Cu. Considerable amounts of C were also present, implying the need for more thorough washing of the synthesis solution to eliminate carbonates, or that the water used for washing was poorly distilled (Vulić and Bošković, 2010). There was also a decrease in the initial molar ratio of (Cu + Mg)/Al, which is probably the result of Mg and Al being elements in the chemical composition of both MMt and LDH, and thereby producing an overlap in the molar ratio. The change in the elements distribution of CuMgAl-LDH/MMt and decrease in the initial molar ratio are very strong proof of the success of structuring LDH with MMt by a co-precipitation method. The EDS spectrum after sorption of Cd^{2+} is illustrated in Fig. 5b. The figure shows the EDS spectrum of LDH/MMt loaded with Cd^{2+} and also that the CuMgAl-LDH/MMt content and elements distribution had changed. This proved the sorption of Cd^{2+} onto CuMgAl-LDH/MMt.

FTIR spectra of MMt, CuMgAl-LDH/MMt before and after Cd^{2+} ion adsorption, is shown in Fig. 6. It shows the existence of functional groups that might be responsible for the adsorption process. Some peaks were seen at 3420, 1635 and 1033 cm^{-1} in MMt, indicating the stretch vibrations of Al–OH, –OH and Si–O–Si respectively (Ahmadi et al., 2020). Also, other peaks were observed at 796, 532, 470 cm^{-1}, which are attributed to Mg–Al–OH, Si–O–Al, and Si–O–Si (Ahmadi et al., 2020; Madejova, 2003). A shown in Fig. 6b, a characteristic band at 3625 cm^{-1} can be ascribed to Al-OH groups located between the octahedral and tetrahedral layers (Madejova, 2003; Shattar et al., 2017). The broad vibrating band at 3444 cm^{-1}, and the weak band at 1634 cm^{-1}, are ascribed to the H—O—H bending vibration of free water and the stretching vibration of –OH groups of interlaminar water molecules in the LDH structure, respectively (Jiang et al., 2019a; Kostic et al., 2018; Madejova, 2003; Mishra et al., 2012). The peaks at 2956 and 2853 cm^{-1} are assigned to the asymmetric C—H and symmetric C—H stretching vibrations (Mishra et al., 2012). The nitrate in the layers of LDH can be observed at a wavenumber of 2359 cm^{-1}(Seddighi et al., 2017). The broad absorption band at 1034 cm^{-1} is ascribed to Si–O stretching vibrations of the tetrahedral-layer (Breen et al., 1995; Madejova, 2003), whereas the vibrating bands at 530 cm^{-1} and 472 cm^{-1} are attributed to Si–O–Al and Si–O–Si groups, respectively. The absorption bands in the range of 650–850 cm^{-1} are attributed to the Al–M − OH (M = Mg and Cu) that are present on the edges of LDH sheets (Hossein Panahi et al., 2017; Mishra et al., 2012). The bands of metal-hydroxide octahedral complexes (M − O, M = Mg and Cu) can be detected at lower wavenumbers in the 520–380 cm^{-1} region (Seddighi et al., 2017). It indicates that the CuMgAl-LDH grew on the MMt, which is consistent with the characterization provided by the XRD (Jiang et al., 2019a). The distinctive bands of the CuMgAl-LDH/MMt structure were clearly detected in the FTIR spectra after Cd^{2+} ion sorption (Fig. 6c), however their intensities were drastically reduced compared to those shown in Fig. 6b. This indicates that the solid particles of the adsorbent maintain their chemical structure throughout the interaction between the solid surfaces and the solution (Khitous et al., 2015). Some peaks behaved differently, with observable shifts in their wavenumbers, indicating that the studied metals had a strong affinity for the functional groups on their surface (Mohammed et al., 2020; Shahid et al., 2021). As shown in Fig. 6c, the intensities of the bands of metal-hydroxide octahedral complexes were significantly changed. This suggests that the mechanism of ion exchange with octahedral ions is responsible for the removal of cadmium ions from the solution (Khitous et al., 2015).

3.2. Parameters affecting Cd^{2+} adsorption

The sorption of Cd^{2+} is affected by several factors including pH, adsorbent dose, agitation speed, particle size, initial Cd^{2+} concentration, and adsorbate–adsorbent contact time.

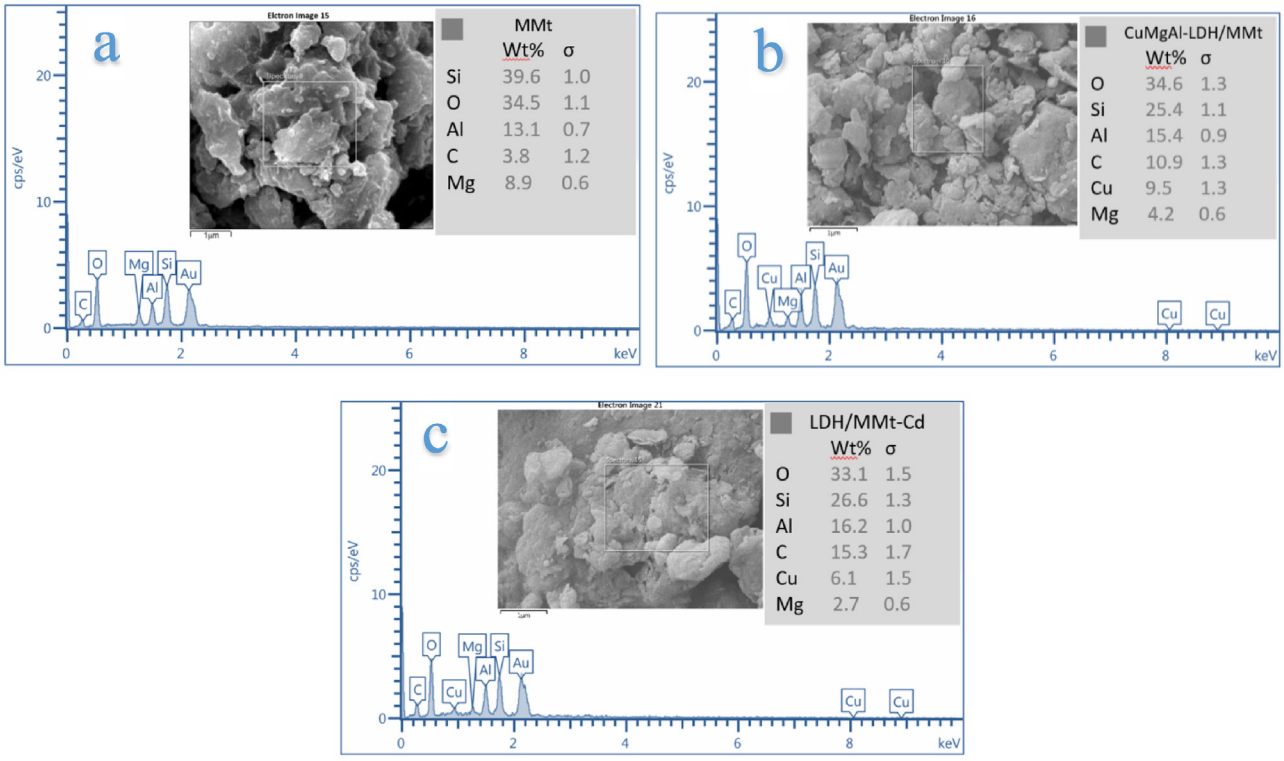

Fig. 5 EDS analysis of (a)CuMgAl-LDH/MMt before adsorption, (b)CuMgAl-LDH/MMt after Cd^{2+} sorption.

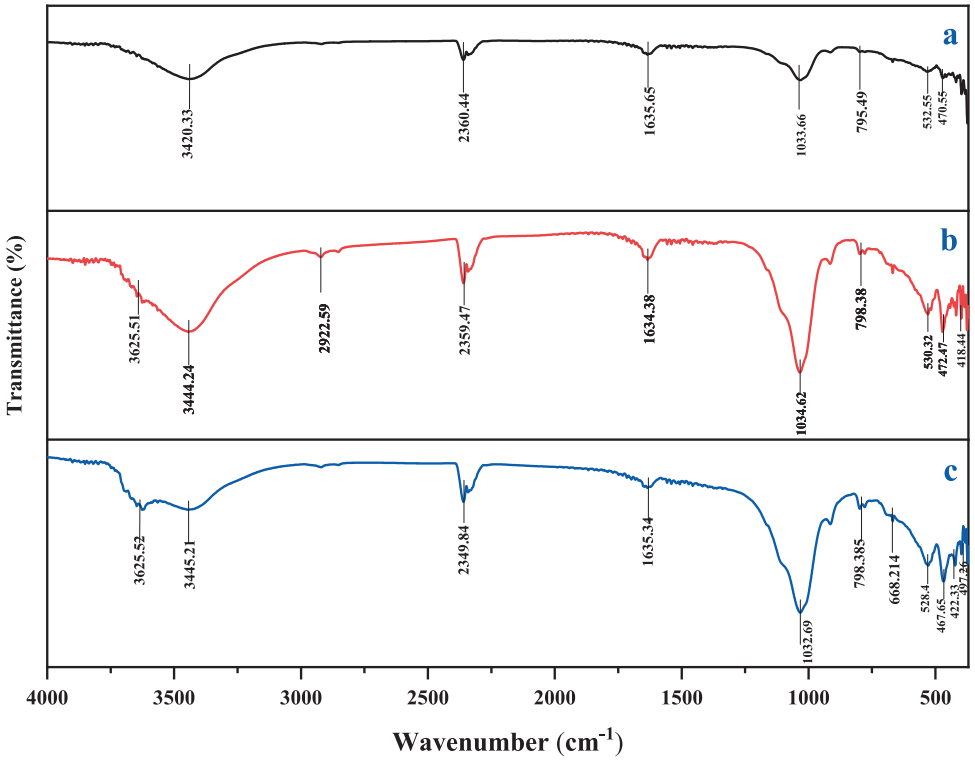

Fig. 6 FTIR of (a) MMt, CuMgAl-LDH/MMt (b) before adsorption, and (c) after Cd^{2+} sorption.

The pH substantially affects both the adsorbent chemistry and surface charge of the LDH-based composites. This greatly influences its tendency toward adsorbent particles, the speciation of ions in the solution, and the conditioning of the adsorption mechanism (Chen et al., 2019; Zubair et al., 2017). In this study, the effect of initial pH (2–8) on the adsorption of 50 ppm of Cd^{2+} on 0.25 g of adsorbent was investigated. The adsorption capacity increased up to a maximum value of 14.3 mg/g at a pH of 5 (see Fig. 7a). As pH increases, the electrostatic attraction, or chemisorption, will occur more readily since the active groups in LDH, such as –OH groups, are gradually deprotonated, accompanied by the negatively charged surface(Seddighi et al., 2017). On the other hand, the adsorption capacity decreased with further increases in pH beyond 5 to 8.0 (12.2 mg/g). This can be attributed to the electrostatic repulsion between the Cd^{2+} species and the CuMgAl-LDH/MMt surface charges, which is influenced by the pH-solution, as well as to the metal complexes lower solubility in higher pH solutions decreasing sufficiently to allow precipitation. The results showed the removal rate of Cd^{2+} was more pH-dependent and that while CuMgAl-LDH/MMt can adsorb Cd^{2+} in acidic, neutral, and basic media, acidic media have the highest removal rate. The pH effect can be explained in terms of the point zero charge (pH_{PZC} = 4.1), which indicates the pH at which the surface of CuMgAl-LDH/MMt is electrically neutral (Nava-Andrade et al., 2021). The pH effect could be explained in terms of the point zero charge (pH_{PZC} = 4.1), which indicates the pH at which the surface of CuMgAl-LDH/MMt is electrically neutral (Nava-Andrade et al., 2021).

When pH < pH_{PZC}, the CuMgAl-LDH/MMt surface is protonated and the adsorbent surface becomes positively charged causing the electrostatic repulsion between Cd^{2+} and the adsorbent surface and it become strongly at the highly alkali media. In contrast, when the pH is greater than pH_{PZC} the surface becomes deprotonated, and its resulting negative charge increases the electrostatic attraction of the binding sites to Cd^{2+}, thereby enabling the surface to adsorb more Cd^{2+} (Mittal, 2021).

The effects of different dosages of CuMgAl-LDH/ MMt (0.05, 0.1, 0.15, 0.2, 0.25, and 0.3 gm/100 ml) on Cd^{2+} adsorption are shown in Fig. 7b. It can be observed that the Cd^{2+} removal efficiency increases from 38.4 % to 77.9 % when the sorbent dose rises from 0.05 to 0.2 g. Furthermore, the high sorbent dosage resulted in a reduced adsorption capacity of CuMgAl-LDH/MMt at an initial Cd^{2+} concentration of 50 ppm. This behavior was most likely caused by the low sorbent dose, which caused the dispersion of CuMgAl LDH/MMt particles in the liquid phase. In this situation, adsorption at the surface was rapidly saturated, showing a high capacity for adsorption. At increased particle concentrations, however, the availability of sites with higher energy declines, and a greater proportion of the lower-energy sites get occupied, resulting in a diminished adsorption capability(Bo et al., 2015). As a result, future experimental of adsorption will use 0.20 g as the effective dose.

As indicated in Fig. 7c, four agitation speeds (100, 150, 200, and 250 rpm) were considered to examine the influence of external diffusion at the optimum pH and CuMgAl-LDH/MMt dose. As agitated speed rose, Cd^{2+} ion removal increased, plateauing at 150 rpm (20.11 mg/g). As the agitation speed increased, the liquid stationary layer around the adsorbent particle decreased. The external diffusion coefficient increases, reducing mass transfer resistance. This increases cadmium's diffusivity from the bulk liquid phase via the boundary layer to the sorbent surface (Evans et al., 2002; Shen and Duvnjak, 2005). Higher agitation speeds may reduce contaminant removal and adsorption time owing to the vortex phenomena (Arif et al., 2022).

The sorbent size also plays a significant role in the sorption process (Vijayaraghavan and Yun, 2008). At optimum pH, agitation speed, and sorbent dose, the influence of three CuMgAl-LDH/MMt particle sizes (87, 122, and 194 μm) on Cadmium ion adsorption was examined (Fig. 7d). As explained in the figure, Cd^{2+} uptake decreased with increasing sorbent particle size, with the smallest particle size (87 μm) yielding the highest cadmium uptake (22.36 mg/g). Smaller particles have greater specific surface areas, more binding sites, and exhibit faster adsorption (Mohammed and Kareem, 2021). Hence, a particle size of 87 μm was used, in conjunction with the other previously established optimal parameters, to examine the effect of initial concentration and contact time.

Fig. 7e and f shows the uptake of CuMgAl-LDH/MMt as a function of different initial Cd^{2+} concentrations and contact time. The uptake of Cd^{2+} (qe) increases from 8.15 to 32.59 mg/g when the initial Cd^{2+} concentration increases from 20 to 70 ppm (Fig. 7e.) This is because at higher concentrations, the driving force increases and overcomes the mass transfer resistance of the sorbate between the liquid phase and the solid phase. The higher uptake is thus attributed to adsorption occurring in a monolayer at a low initial concentrations but changing to a multilayer at a high initial concentrations (Mittal, 2021; Nava-Andrade et al., 2021). The curves also illustrated a rapid increase in the adsorption of Cd^{2+} at the first stage. After that, the adsorption process increased slowly until equilibrium was reached at minute 120. This behavior can be described as follows: in the first 30 min, the adsorbent has more active sites and most adsorption sites become saturated. and the rest of them are hard to occupy owing to the repulsive force between the bulk phases and solid sorbate molecules (Jiang et al., 2019a)(Mohammed and Kareem, 2021).

From the above results, it can be concluded that under optimal conditions for the sorption of cadmium ions on a CuMgAl-LDH/MMt adsorbent, the maximum uptake for Cd^{2+} ion is 32.6 mg/g. Using these optimal conditions, Cd^{2+} ion adsorption of MMt and CuMgAl-LDH were investigated and the uptake was 10.7 mg/g and 12.5 mg/g, respectively. Therefore, CuMgAl-LDH/MMt can be considered a superior adsorbent for the removal of Cd^{2+} in aqueous solutions.

Cd^{2+} in aqueous solutions.

3.3. The effect of ionic strength and Co-existing

The existence of soluble ions may have a competing effect on the adsorption site (Johnston et al., 2021). The effect of ionic strength was investigated by adding different concentrations of NaCl (0.01, 0.1, 0.5, and 1 mol/l) to 50 ppm Cd^{2+} solutions at the previously determined optimum conditions. Fig. 8a shows that there was no significant effect of NaCl salt, at a concentration of 0.01 mol/L, on the uptake of Cd^{2+} ions, which indicates the formation of inner-sphere complexes

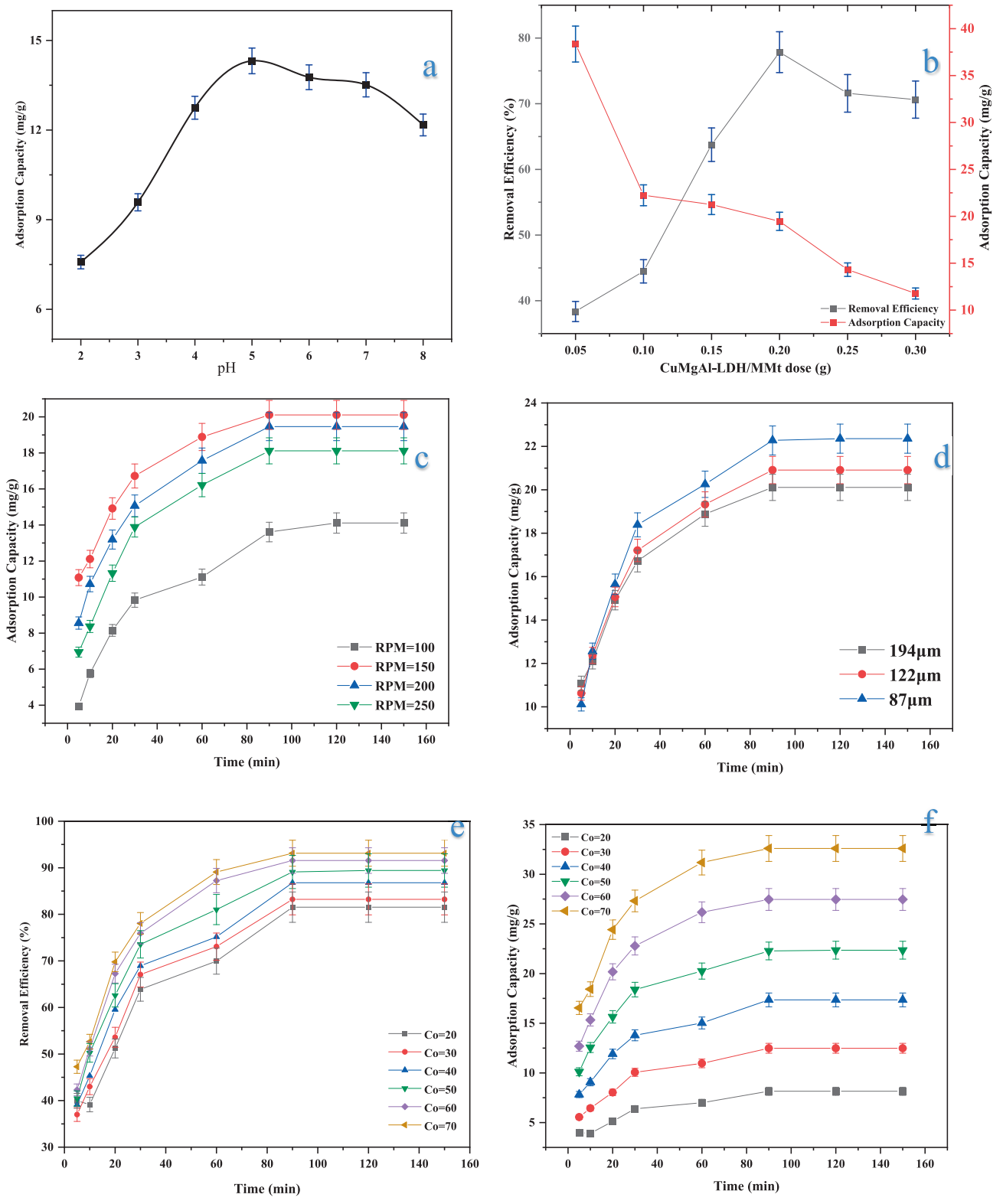

Fig. 7 Effect of expremental conditions on Cd^{2+} sorption onto CuMgAl-LDH/MMt. (a) pH-solution at Co = 50, dose = 0.25 g, rpm = 200, and particle size = 194 µm; (b) CuMgAl-LDH/MMt dose at pH = 5, Co = 50, rpm = 200, and particle size = 194 µm; (c) agitation speed at pH = 5, Co = 50, dose = 0.2g, and particle size = 194 µm; (d) CuMgAl-LDH/MMt particle size at pH = 5, Co = 50, dose = 0.2g, and rpm = 150; and (e) initial Cd^{2+} concentration at pH = 5, dose = 0.2g, and rpm = 150, and 87 µm,

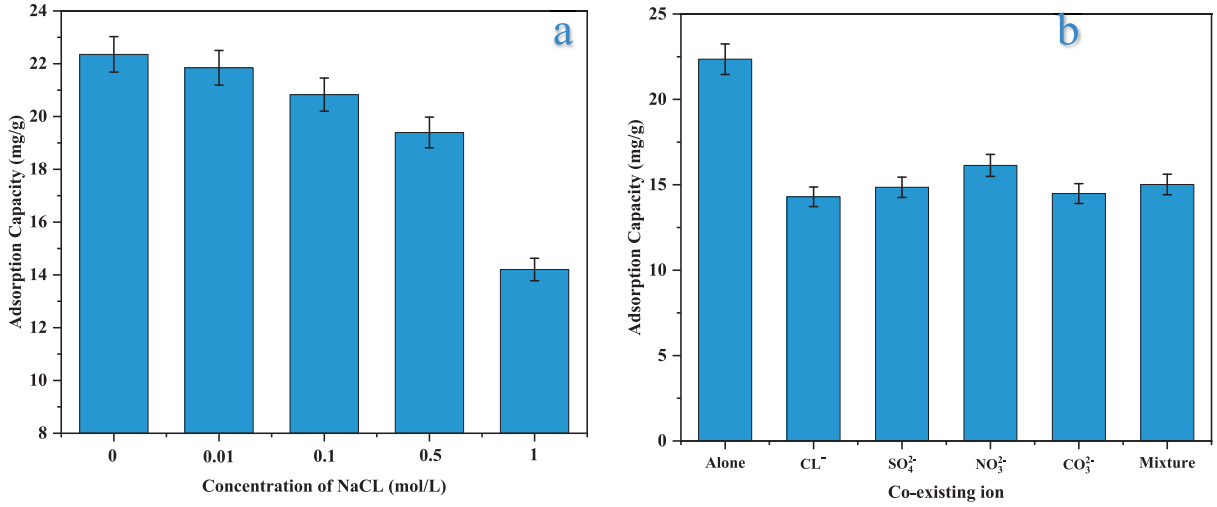

Fig. 8 Effect of (a) ionic-strength, (b) Co-existing ions, on Cd^{2+} sorption at pH = 5, dose = 0.2 g, and rpm = 150, 87 μm, and Co = 50 ppm, and t = 120 min.

(Sahu et al., 2019). The trapping of Cd^{2+} decreased gradually with the augmenting concentration of the NaCl salt, implying that the sorption was governed not by inner-sphere but by outer-sphere surface complexation (Wang et al., 2017).

Further experiments were carried out, also at previously determined optimum conditions, to assess the elimination of 50 ppm of Cd^{2+} in the presence of 50 ppm of common interfering ions in water such as nitrate, chloride, sulfate, carbonate, and sulfite. The interference of competing anions on Cd^{2+} adsorption follows the decreasing order $NO_3^{2-} < SO_4^{2-} < CO_3^{2-} < Cl^-$ indicating that nitrate has a relatively low impact on its removal (see Fig. 8b), which could be attributed to both charge density and the hydrated ionic radius. The distribution coefficient (K_d) of Cd^{2+} (ml/g) was calculated using Eq. (6), as it is important to know the affinity of the adsorbent toward the adsorbate molecule. The K_d values for the Cd^{2+} were in the range of 0.67–4.23 × 10^3 ml/g. The high K_d values for LDH/MMt indicates the great affinity of the material toward Cd^{2+} (Foroutan et al., 2022; Sahu et al., 2019).

$$K_d = \left(\frac{C_o - C_e}{C_e}\right)\frac{V}{W} \tag{6}$$

Where C_0 and Ce are the initial and equilibrium concentration of Cd^{2+} (mg/l), respectively; m is the mass of CuMgAl-LDH/MMt (g), and V is the volume of solute (l).

From this section, it can be concluded that the existence of high concentration soluble ions effect on adsorption (Low selectivity) and can be limited of using it.

3.4. Effect of temperature and adsorption thermodynamics

The results for the removal efficiency of Cd^{2+} as a function of solution temperature are shown in Fig. S1a. The removal efficiency dropped from 89.42 % to 73.16 % as the temperature was raised from 25 to 40 °C, owing to solute mobility increasing from the solid to the bulk phase. This causes a deactivation of the solid surfaces or the destruction of some binding sites, as well as desorption, which takes place in preference to sorption (Mohammed and Kareem, 2019).

The concept of thermodynamics presumes that entropy change considered a driving force for the adsorption in an isolated system (Shattar et al., 2017). The relationship of adsorption temperature and kinetic parameters can be analyzed by determining thermodynamic parameters (standard entropy change (ΔS^o), standard enthalpy change (ΔH^o), and Gibbs free energy change (ΔG^o)), using the following equations (Amin et al., 2020; Santos et al., 2017):

$$\Delta G^o(kJ/mol) = -RTln(K_T) \tag{7}$$

$$ln(K_T) = \frac{\Delta S^o}{R} - \frac{\Delta H^o}{RT} \tag{8}$$

$$\Delta G^o = \Delta H^o - \Delta S^o \tag{9}$$

K_T is the equilibrium constants (the ratio of Cd^{2+} concentration in the solid and liquid phase), R is the universal gas constant (8.314 J/mol K), and T is the temperature (K). Thermodynamic studies are typically conducted at a range of temperatures (298,303, 308, and 313 K) in order to analyze experimental data. The linear graphs of ln K_2 vs 1/T are shown in Fig. S1b, and the thermodynamic parameters for Cd^{2+} sorption (ΔS^o, ΔH^o, and ΔG^o) are provided in Table 2. The negative value of enthalpy change (ΔH^o) in Table 2 indicates the exothermic nature of the adsorption process of Cd^{2+} on CuMgAl-LDH/MMt. This implies that increases in temperature reduced the adsorption capacity of the adsorbent (hence

Table 2 Thermodynamic parameters of cd^{2+} sorption.

ΔT	ΔG°	ΔS°	ΔH°
K	KJ/mol	KJ/mol.K	KJ/mol
298	−3.02	−185	−57.9
303	−1.59		
308	−0.771		
313	−0.225		

reduced K_T values) (Zubair et al., 2018)(Mohammed et al., 2020), while the negative value of the energy change, ΔG^o, denotes the spontaneity of adsorption (George and Saravanakumar, 2018). Moreover, the negative values of ΔS^o designated higher order of reactions during the sorption process, which could be attributed to the adhesion of sorbate to the adsorbent, thereby reducing the degrees of freedom of the system (Shan et al., 2014).

3.5. Kinetics of Cd^{2+} adsorption

Models of adsorption kinetics are important for fitting equilibrium data for adsorption because they help determine rate-limiting steps and the interaction mechanism between the adsorbate and the adsorbent (Mittal, 2021). Four kinetics models were used to predict the order and rate of the adsorption process. The pseudo-first-order model (PFO), pseudo-second-order model (PSO), Elovich model (EIH), and intra-particle diffusion model (IPD) assume that the adsorption rate is generally directly related to the equilibrium uptake difference and time, and expressed mathematically in Eqs. 10–13 (Chao et al., 2018; Li et al., 2021; Shen et al., 2016).

$$\ln(q_e - q_t) = \ln q_e - k_1.t \tag{10}$$

$$\frac{t}{q_t} = \frac{t}{q_e} + \frac{1}{q_e^2.k_2} \tag{11}$$

$$q_t = \frac{1}{\beta}\ln(1 + \alpha.\beta.t) \tag{12}$$

$$q_t = K_{id}.t^{0.5} + C \tag{13}$$

Where: q_e and q_t are the uptake rates of Cd^{2+} (mg/g) at equilibrium and time t, respectively; k_1 is the constant of the PFO (1/min) and k_2 is the constant of the PSO (g/mg.min); α is the initial rate of adsorption(mg/g.min); β is the constant of desorption (mg/g); K_{id} is the constant of intra-particle diffusion rate (mg/g.min $^{(1/2)}$) and C is the constant of intra particle diffusion (mg/g).

From the pseudo-second-order model at time at $t \rightarrow 0$, the initial rate of adsorption δ is obtained as follows: Eq. (14) and Fig. s2b (Mohammed and Kareem, 2019).

$$\delta = K_2.q_e^2 \tag{14}$$

Where: δ is the initial adsorptive rate(mg/g. min), k_2 is the constant of PSO (g/mg.min).

The regression coefficients and slopes of the straight lines in the plots of ln (qe – qt) versus time (PFO), t/qt versus time (PSO), q_t versus $Ln(t)$ (EIH), and q_t versus $t^{0.5}$ (IPD), can be used to infer the order and rate constant of the adsorption process., respectively, The fitted lines for each model are depicted in Fig. S2a-c. Table 3 shows the kinetic parameters (k_1, k_2, α) and the correlation coefficients (R^2) that correspond to these values. The value of R^2 for the PSO model was greater than those of the other models, and closer to 1. In addition to this, the calculated adsorption capacity $q_{e,cal}$ of the pseudo-second-order model (PSO) agreed with the experimental adsorption capacity $q_{e,Exp.}$. Thus, it was concluded that the PSO adsorption mechanism was dominant and that chemisorption process seemed to control the overall rate of the Cd^{2+} adsorption process (Hu et al., 2016).

The intra-particle diffusion Kinetic model (IPD) is also used to explain diffusion mechanisms. The IPD model parameters are listed in Table 4, and Fig. s2d shows the linear fit of the IPD model. As the figure explains, the entire kinetic process of Cd^{2+} diffusion is controlled by three adsorption mechanisms. The first phase (bulk-diffusion) is immediate adsorption, which happens on the exterior surface of the solid particles and takes about three minutes. This phase is induced by the large number of active adsorption sites as well as the high initial concentration of Cd^{2+}, thus giving it enough driving force to diffuse rapidly to the adsorbent surface (Lei et al., 2017). The second phase (gradual-adsorption) primarily addresses the intraparticle diffusion within the CuMgAl-LDH/MMt adsorbent (Shin and Kim, 2016). K_{id2} is related to pore volume and pore size distribution (Hu et al., 2020). The third phase is the equilibrium stage, in which the molecules are adsorbed at the interior surface of CuMgAl-LDH/MMt particles, and because of low Cd^{2+} concentrations, intraparticle diffusion slows until equilibrium is reached (Hu et al., 2020; Shin and Kim, 2016). Fitting the experimental data to the IPD model suggests that intraparticle diffusion may be the rate-limiting step in Cd^{2+} adsorption.

3.6. Adsorption isotherm models

Isotherm models are essential to predict the complete adsorption behavior in practical applications and to calculate the maximum contaminant removal from polluted water at a constant temperature. To investigate the precise adsorption mechanism and compute the adsorption capacity, a non-linear optimization Langmuir (Eq. (15)), Freundlich (Eq. (16)), Tem-

Table 3 PFO, PSO, and EIH parameters and correlation coefficients for sorption of Cd^{2+}.

C_o	$q_{e,\ Exp.}$	PFO				PSO				EIH				
		$q_{e,cal.}$	K_1	R^2	X^2	$q_{e,cal.}$	K_2	R^2	X^2	δ	α	β	R^2	X^2
mg/L	mg/g	mg/g	1/min			mg/g	g/mg.min			mg/g.min	mg/g.min	mg/g		
20	8.15	12.1	8.15×10^{-4}	0.809	1.27	8.83	0.0101	0.996	0.052	0.78	0.691	3.24	0.951	7.48
30	12.5	23.5	9.78×10^{-4}	0.800	5.17	13.5	0.00713	0.997	0.071	1.29	0.442	4.78	0.972	12.4
40	17.4	18.1	5.85×10^{-4}	0.902	0.026	18.6	0.00535	0.997	0.089	1.86	0.326	7.43	0.978	13.4
50	22.4	19.8	6.01×10^{-4}	0.914	0.331	23.8	0.00482	0.999	0.091	2.74	0.260	11.5	0.978	10.3
60	27.5	33.2	8.39×10^{-4}	0.917	0.975	29.2	0.00441	0.999	0.099	3.76	0.213	15.5	0.964	9.34
70	33.3	9.53	9.75×10^{-4}	0.886	3.98	34.5	0.00408	0.999	0.036	4.84	0.191	24.8	0.953	2.91

Table 4 Parameters and correlation coefficients of IPD model for sorption of Cd^{2+}.

Co	$q_{e,Exp.}$	K_{id1}	K_{id2}	K_{id3}	C_1	C_2	C_3	$(R_1)^2$	$(R_2)^2$	$(R_3)^2$
20	5.96	1.79	0.769	0.289	0	1.91	4.92	1	0.891	0.862
30	9.87	2.48	1.37	0.393	0	2.27	8.09	1	0.976	0.864
40	13.6	3.49	1.89	0.583	0	3.40	10.8	1	0.993	0.862
50	18.2	4.52	2.53	0.623	0	4.49	15.4	1	0.999	0.874
60	22.2	5.68	3.19	0.676	0	5.49	20.1	1	0.995	0.788
70	26.7	7.40	3.50	0.76	0	8.24	24.3	1	0.983	0.785

kin (Eq. (17)), and Dubinin-Radushkevich (D-R) (Eq. (18)) isotherms models were used to analyze isothermal data.

$$q_e = K_f.C_e^{(\frac{1}{n})} \tag{15}$$

$$q_e = \frac{K_L.q_{max}.C_e}{1 + K_L.C_e} \tag{16}$$

$$q_e = B.(A_T.C_e),\ B = \frac{RT}{b_T} \tag{17}$$

$$q_e = q_m \exp\left(-K_{DR}\,\varepsilon^2\right),\ \varepsilon = RT\ln(1 + \frac{1}{C_e}) \tag{18}$$

Where: qe is an adsorbed amount under equilibrium condition (mg/g); q_{max} a maximum uptake of sorbate (mg/g); K_f a constant of the Freundlich isotherm (m/g)(l/mg)$^{1/n}$; K_L a constant of the Langmuir isotherm (l/mg); b_T is the Temkin isotherm constant related to the heat of adsorption (J/mol); and A_T an is equilibrium binding constant (l/g); K_{DR} is a constant of D-R (mol/J)^2; ε is a potential of Polanyi; Ce the concentration of the sorbate at equilibrium (mg/l), and n is the intensity of the Freundlich adsorption parameter (which indicates the existence of adsorption driving forces and the degree of surface heterogeneity). A non-linear regression analysis was performed using the Solver add-in in Microsoft Excel to calculate the parameters of each model. This enabled the best fitting model to be selected (Ahmed et al., 2017; Blaisi et al., 2018; Mittal, 2021; Mohammed and Kareem, 2019; Nava-Andrade et al., 2021; Zubair et al., 2017). The determined constants and variables for the sorption isotherms of Cd^{2+} on the CuMgAl-LDH/MMt surface study are presented in Table 5. The obtained R^2 value of CuMgAl-LDH/MMt composites for the Langmuir isotherm was 0.9933, which was lower than that of the Freundlich isotherm. This revealed that the Langmuir isotherm did not adequately describe Cd^{2+} sorption on CuMgAl-LDH/MMt. The Freundlich isotherm model assumes multilayer adsorption at heterogeneous surfaces and the nonuniform energy distribution to the active adsorbent site occurs(Dinari and Neamati, 2020).

If the value of 1/n is less than unity as in Table 5, it indicates the heterogeneity of site energies as well as higher adsorption intensity (Mu'azu et al., 2018). The maximum adsorption capacity of the CuMgAl-LDH/MMt was 174.87 mg/g, which was higher than other maximum adsorption capacities reported in previous studies and listed in Table 6. Despite the fact that there are many excellent materials used as adsorbents based LDH in Cd2 + sorption, CuMgAl-LDH/MMt has superior sorption properties for Cd2 + ions when compared to the other adsorbents.

In addition, the Langmuir, or equilibrium, parameter (R_L) is the most important parameter of the Langmuir isotherm and must be considered to estimate the favourability and unfavourability of the adsorption process (Alnasrawi et al., 2022; Shattar et al., 2017).

$$R_L = \frac{1}{1 + K_L C_0} \tag{19}$$

Table 5 Langmuir, Freundlich, Sips, Temkin, and D-R parameters and correlation coefficients for Cd^{2+} sorption.

Isotherm	Parameter	
Langmuir	q_{max}, (mg/g)	175
	K_L, (l/mg)	0.0267
	R^2	0.993
	X^2	0.0069
	R_L	0.428
Freundlich	K_f, (mg/g)(L/mg) $^{1/n}$	6.02
	1/n	0.777
	R^2	0.999
	X^2	0.0032
Temkin	b_T (J/mol)	0.235
	A_T, (l/g)	0.921
	R^2	0.966
	X^2	1.53
D-R	q_s, (mg/g)	59.4
	$K_{DR\times}10^{-6}$, (mol^2/J^2)	6.34
	E, (KJ/mol)	2.8
	R^2	0.969
	X^2	1.47

Table 6 Comparison of maximum sorption capacity of Cd^{2+} with previous study.

adsorbate	q_m(mg/g)	Ref.
KB/LDH	25.6	(Tan et al., 2019)
Mg–Fe-LDH-RHA	28.9	(Yu et al., 2018)
SDBS-Citrate-LDH	41	(Li et al., 2015)
magneticFe_3O_4-Mg/Al-CO_3-LDH	45.6–54.7	(Shan et al., 2015)
Fe/Mn/Mg-LDH	59.9	(Zhou et al., 2018)
LDH-Cl	61	(González et al., 2015)
MgAl-Cys-LDH	93.1	(Zhang et al., 2020)
CS-LDH	141	(Lyu et al., 2018)
Calcined Mg/Fe–LDH	164	(Puzyrnaya et al., 2020)
CuMgAl-LDH/MMt	175	In the present study

The process is unfavorable if $R_L > 1$, favorable if $0 < R_L < 1$, linear if $R_L = 1$, and irreversible if $R_L = 0$. These results imply that the isotherm adsorption is controlled by the Langmuir model and that Cd^{2+} species adsorption is a favorable process ($0 < R_L < 1$ calculated from Eq. (19)).

The Temkin isotherm is used to explore the impact of indirect adsorbate–adsorbate interactions on the sorption system, whereas the D-R model determines if the sorption process is chemical or physical. Calculation of the Temkin model parameters showed that the interaction of Cd^{2+} with CuMgAl-LDH/MMt composite surfaces is weak, and most probably a physical sorption process. The mean free energy of surface adsorption for Cd^{2+} attraction of 2.8 kJ/mol confirm a physical sorption process (E < 8 kJ/mol) (Foroutan et al., 2021b, 2020b).

It can be concluded that isotherm adsorption is controlled by the Freundlich adsorption isotherm model, as well as that the adsorption of Cd species by the adsorbent is a favorable process (because the calculated R_L was in the range of 0 and 1).

3.7. Desorption of Cd^{2+} and reusability of CuMgAl-LDH/MMt nonabsorbent

To investigate the reusability of LDH/MMt, five successive cycles of regeneration (sorption–desorption) were carried out. The resorption process is tested by adding 0.5 g of spent CuMgAl-LDH/MMt to 100 ml of 0.2 M NaOH and another to 100 ml 0.2 M of HCL. The mixture was stirred for 180 min, filtered, washed three times with distilled water, and dried in the oven. This process was repeated five times. The adsorption capacity of the regenerated adsorbent in each cycle is calculated using Eq. (2). As displayed in Fig. 9, the trapping of Cd^{2+} dropped to 14.96 mg/g after five cycles of regeneration of adsorbent with the NaOH solution. The adsorption capacity also decreased to 7.06 mg/g after five cycles of regenerating the adsorbate with the HCL solution. The reduced uptake of reused CuMgAl-LDH/MMt was most likely attributable to the nanocomposite's decreasing crystallinity (Yuan et al., 2013). As stated in Section 3.2, increasing the solution pH resulted in drastically reduced cadmium uptake by the CuMgAl-LDH/MMt. These results demonstrate that relatively alkaline conditions ($pH > pH_{PZC}$) can facilitate cadmium desorption from exhausted adsorbent. Thus, the cadmium desorption process from cadmium-loaded CuMgAl-LDH/MMt was more efficient. These outcomes indicate that the recently developed nanocomposites have a high potential for recycling, resulting in cost savings and diminished environmental impact (Du et al., 2019).

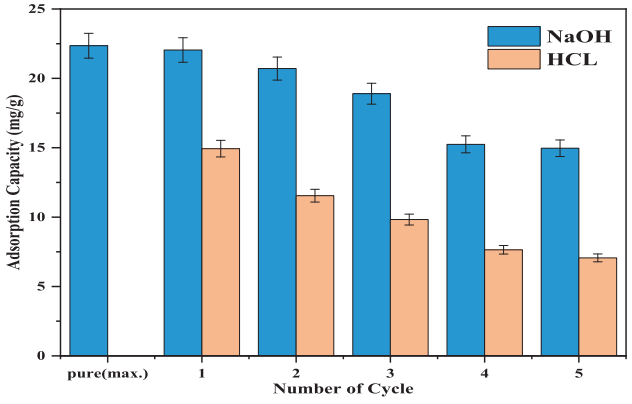

Fig. 9 Regeneration of cumgal-ldh/mmt samples (at ph = 5, dose = 0.2 g, and rpm = 150, and 87 μm).

4. Conclusions and future directions

In the present work, a CuMgAl layered double hydroxide based nanocomposite was produced using a co-precipitation technique to prepare a large specific surface area Montmorillonite supported CuMgAl-LDH nanocomposite. The synthesized CuMgAl-LDH/MMt characterized using TEM, XRD, BET, SEM/EDX, and FTIR to investigate its ability to eliminate cadmium from wastewater in batch adsorption systems with different operating parameters. Consequences display that the adsorption of Cd^{2+} on the CuMgAl-LDH/MMt adsorbent is intensely pH-dependent. The experimental data were a better fit to the Freundlich isotherm model than the Langmuir, indicating multilayered adsorption. Thermodynamic analysis showed that Cd^{2+} adsorption onto CuMgAl-CuMgAl-LDH/MMt was spontaneous and endothermic in nature. Cd^{2+} adsorption was well described by the pseudo-second order kinetic model. The obtained results proved that CuMgAl-LDH/MMt adsorbent was found to be an efficient and low-cost adsorbent for the elimination of heavy metal ions from wastewater. Furthermore, it is easily regenerated by 0.2 NaOH and usable for several cycles.

The widespread application of LDH in the removal of pollutants from aqueous solutions is almost fixed. New composites, based on LDH, have considerable potential, but the research is also facing new challenges.

1. A suggestion for lowering the investment costs in the production of LDH-nanocomposite, is to investigate the synthesis of CuMgAl-LDH using green chemistry.
2. The regeneration process effectively mitigates secondary pollution problems. Choosing green eluents and exploring desorption conditions for the regeneration process should be remarked in prospective publications.
3. Future research should be conducted to determine how magnetic CuMgAl-LDH/MMt can be obtained as iron oxides help to improve pore quality.
4. More studies should be conducted to examine the removal of pollutants like pharmaceutical drugs, pesticides, hazardous organic dyes, persistent organic contaminants, and explosive compounds by CuMgAl-LDH/MMt.

Declaration of Competing Interest

The authors declare that they have no known competing financial interests or personal relationships that could have appeared to influence the work reported in this paper.

Acknowledgments

The authors express their gratitude to the University of Baghdad and University of Kerbala for the scientific support given to accomplish this study.

Appendix A. Supplementary material

Supplementary data to this article can be found online at https://doi.org/10.1016/j.arabjc.2022.104471.

References

Ahmadi, A., Foroutan, R., Esmaeili, H., Jamaleddin, S., Hemmati, P. S., Ramavandi, B., 2020. Montmorillonite clay/starch/CoFe2O4 nanocomposite as a superior functional material for uptake of cationic dye molecules from water and wastewater. Mater. Chem. Phys. 284, 126088 Contents. https://doi.org/https://doi.org/10.1016/j.matchemphys.2022.126088.

Ahmed, M.A., Brick, A.A., Mohamed, A.A., 2017. An efficient adsorption of indigo carmine dye from aqueous solution on mesoporous Mg/Fe layered double hydroxide nanoparticles prepared by controlled sol-gel route. Chemosphere 174, 280–288. https://doi.org/10.1016/j.chemosphere.2017.01.147.

Ai, L., Zhou, Y., Jiang, J., 2011. Removal of methylene blue from aqueous solution by montmorillonite / CoFe 2 O 4 composite with magnetic separation performance. Desalination 266, 72–77. https://doi.org/10.1016/j.desal.2010.08.004.

Almeida, C.A.P., Debacher, N.A., Downs, A.J., Cottet, L., Mello, C. A.D., 2009. Journal of colloid and interface science removal of methylene blue from colored effluents by adsorption on montmorillonite clay. J. Colloid Interface Sci. 332, 46–53. https://doi.org/10.1016/j.jcis.2008.12.012.

Alnasrawi, F.A.M., Kareem, S.L., Mohammed Saleh, L.A., 2022. Adsorption of methylene blue from aqueous solution using different types of activated carbon. J. Appl. Water Eng. Res. https://doi.org/10.1080/23249676.2022.2120918.

Amin, M.T., Alazba, A.A., Shafiq, M., 2020. LDH of NiZnFe and its composites with carbon nanotubes and data-palm biochar with efficient adsorption capacity for RB5 dye from aqueous solutions : isotherm, kinetic, and thermodynamics studies. Curr. Appl. Phys. https://doi.org/10.1016/j.cap.2020.07.005.

Arif, M., Shahid, M., Irfan, A., Nisar, J., Wang, X., Batool, N., Ali, M., Farooqi, Z., Begum, R., 2022. Extraction of copper ions from aqueous medium by microgel particles for in-situ fabrication of copper nanoparticles to degrade toxic dyes. De Gruyter 236, 1219–1241. https://doi.org/10.1515/zpch-2022-0038.

Begum, R., Farooqi, Z.H., Xiao, J., Ahmed, E., Sharif, A., Irfan, A., 2021. Crosslinked polymer encapsulated palladium nanoparticles for catalytic reduction and Suzuki reactions in aqueous medium. J. Mol. Liq. 338,. https://doi.org/10.1016/j.molliq.2021.116780 116780.

Blaisi, N.I., Zubair, M., Ali, S., Kazeem, T.S., 2018. Date palm ash-MgAl-layered double hydroxide composite : sustainable adsorbent for effective removal of methyl orange and eriochrome black-T from aqueous phase. Environ. Sci. Pollut. Res. 25, 34319–34331. https://doi.org/10.1007/s11356-018-3367-2.

Bo, L., Li, Q., Wang, Y., Gao, L., Hu, X., Yang, J., 2015. One-pot hydrothermal synthesis of thrust spherical Mg-Al layered double hydroxides/MnO2 and adsorption for Pb(II) from aqueous solutions. J. Environ. Chem. Eng. 3, 1468–1475. https://doi.org/10.1016/j.jece.2015.05.023.

Breen, C., Madejová, J., Komadel, P., 1995. Characterisation of moderately acid-treated, size-fractionated montmorillonites using IR and MAS NMR spectroscopy and thermal analysis. J. Mater. Chem. 5, 469–474. https://doi.org/10.1039/JM9950500469.

Bukhtiyarova, M.V., 2019. A review on effect of synthesis conditions on the formation of layered double hydroxides. Solid State Chem. 269, 494–506. https://doi.org/10.1016/j.jssc.2018.10.018.

Cao, Y., Li, G., Li, X., 2016. Graphene/layered double hydroxide nanocomposite: properties, synthesis, and applications. Chem. Eng. 292, 207–223. https://doi.org/10.1016/j.cej.2016.01.114.

Chao, H.P., Wang, Y.C., Tran, H.N., 2018. Removal of hexavalent chromium from groundwater by Mg/Al-layered double hydroxides using characteristics of in-situ synthesis. Environ. Pollut. 243, 620–629. https://doi.org/10.1016/j.envpol.2018.08.033.

Charerntanyarak, L., 1999. Heavy metals removal by chemical coagulation and precipitation. Water Sci. Technol. 39, 135–138. https://doi.org/10.1016/S0273-1223(99)00304-2.

Chen, D., Li, Y., Zhang, J., Zhou, J., Guo, Y., Liu, H., 2012. Magnetic Fe3O4/ZnCr-layered double hydroxide composite with enhanced adsorption and photocatalytic activity. Chem. Eng. 185–186, 120–126. https://doi.org/10.1016/j.cej.2012.01.059.

Chen, L., Xu, H., Xie, J., Liu, X., Yuan, Y., Liu, P., Qu, Z., Yan, N., 2019. [SnS4]4- clusters modified MgAl-LDH composites for mercury ions removal from acid wastewater. Environ. Pollut. 247, 146–154. https://doi.org/10.1016/j.envpol.2018.12.009.

Dang, H.H., Nguyen, D.T.C., Nguyen, T.T., Nguyen, T.T.T., Vo, D.-V.-N., Nguyen, T.D., Lee, T., Tran, T.V., 2020. Zeolitic-imidazolate framework-derived N-self-doped porous carbons with ultrahigh theoretical adsorption capacities for tetracycline and ciprofloxacin. J. Environ. Chem. Eng. 9,. https://doi.org/10.1016/j.jece.2020.104938 104938.

Daniel, S., Thomas, S., 2020. Layered double hydroxides: fundamentals to applications, Layered Double Hydroxide Polymer Nanocomposites. Elsevier Ltd. https://doi.org/10.1016/b978-0-08-101903-0.00001-5.

Dinari, M., Neamati, S., 2020. Surface modified layered double hydroxide/polyaniline nanocomposites: synthesis, characterization and Pb2+ removal. Colloids Surf. A Physicochem. Eng. Asp. 589,. https://doi.org/10.1016/j.colsurfa.2020.124438 124438.

Du, L., Wang, X., Liu, T., Li, J., Wang, J., Gao, M., Wang, H., 2019. Magnetic solid-phase extraction of organophosphorus pesticides from fruit juices using NiFe2O4@polydopamine@Mg/Al-layered double hydroxides nanocomposites as an adsorbent. Microchem. J. 150,. https://doi.org/10.1016/j.microc.2019.104128 104128.

Dubey, S., Banerjee, S., Upadhyay, S.N., Sharma, C., 2017. Application of common nano-materials for removal of selected metallic species from water and wastewaters: a critical review Shikha. J. Mol. Liq. 240, 656–677. https://doi.org/10.1016/j.molliq.2017.05.107.

Evans, J.R., Davids, W.G., MacRae, J.D., Amirbahman, A., 2002. Kinetics of cadmium uptake by chitosan-based crab shells. Water Res. 36, 3219–3226. https://doi.org/10.1016/S0043-1354(02)00044-1.

Foroutan, R., Mohammadi, R., MousaKhanloo, F., Sahebi, S., Ramavandi, B., Kumar, P.S., Vardhan, K.H., 2020a. Performance of montmorillonite/graphene oxide/CoFe2O4 as a magnetic and recyclable nanocomposite for cleaning methyl violet dye-laden wastewater. Adv. Powder Technol. 31, 3993–4004. https://doi.org/10.1016/j.apt.2020.08.001.

Foroutan, R., Mohammadi, R., Peighambardoust, S.J., Jalali, S., Ramavandi, B., 2020b. Application of nano-silica particles generated from offshore white sandstone for cadmium ions elimination from aqueous media. Environ. Technol. Innov. 19,. https://doi.org/10.1016/j.eti.2020.101031 101031.

Foroutan, R., Peighambardoust, S.J., Hemmati, S., Ahmadi, A., Falletta, E., Ramavandi, B., Bianchi, C.L., 2021a. Zn2+ removal from the aqueous environment using a polydopamine/hydroxyapatite/Fe3O4 magnetic composite under ultrasonic waves. RSC Adv., 27309–27321 https://doi.org/10.1039/d1ra04583k.

Foroutan, R., Peighambardoust, S.J., Hemmati, S., Khatooni, H., Ramavandi, B., 2021b. Preparation of clinoptilolite/starch/CoFe2O4 magnetic nanocomposite powder and its elimination properties for cationic dyes from water and wastewater. Int. J. Biol. Macromol. 189, 432–442. https://doi.org/10.1016/j.ijbiomac.2021.08.144.

Foroutan, R., Peighambardoust, S.J., Mohammadi, R., Peighambardoust, S.H., Ramavandi, B., 2022. Cadmium ion removal from aqueous media using banana peel biochar/Fe3O4/ZIF-67. Environ. Res. 211,. https://doi.org/10.1016/j.envres.2022.113020 113020.

George, G., Saravanakumar, M.P., 2018. Facile synthesis of carbon-coated layered double hydroxide and its comparative characterisation with Zn-Al LDH: application on crystal violet and malachite green dye adsorption—isotherm, kinetics and Box-Behnken design. Environ. Sci. Pollut. Res. 25, 30236–30254. https://doi.org/10.1007/s11356-018-3001-3.

González, M.A., Pavlovic, I., Barriga, C., 2015. Cu(II), Pb(II) and Cd (II) sorption on different layered double hydroxides. a kinetic and thermodynamic study and competing factors. Chem. Eng. 269, 221–228. https://doi.org/10.1016/j.cej.2015.01.094.

Gu zi, A.J.J. and P.X., 2015. Hierarchical layered double hydroxide nanocomposites: structure, synthesis and applications. Chem. Commun. 3024–3036. https://doi.org/10.1039/C4CC07715F.

Hossein Panahi, F., Peighambardoust, S.J., Davaran, S., Salehi, R., 2017. Development and characterization of PLA-mPEG copolymer containing iron nanoparticle-coated carbon nanotubes for controlled delivery of Docetaxel. Polymer (Guildf) 117, 117–131. https://doi.org/10.1016/j.polymer.2017.03.084.

Hoyo, C.D., 2007. Layered double hydroxides and human health : an overview ✠. Appl. Clay Sci. 36, 103–121. https://doi.org/10.1016/j.clay.2006.06.010.

Hu, H., Wageh, S., Al-Ghamdi, A.A., Yang, S., Tian, Z., Cheng, B., Ho, W., 2020. NiFe-LDH nanosheet/carbon fiber nanocomposite with enhanced anionic dye adsorption performance. Appl. Surf. Sci. 511,. https://doi.org/10.1016/j.apsusc.2020.145570 145570.

Hu, W., Wu, X., Jiao, F., Yang, W., Zhou, Y., 2016. Preparation and characterization of magnetic Fe3O4@sulfonated β-cyclodextrin intercalated layered double hydroxides for methylene blue removal. Desalin. Water Treat. 57, 25830–25841. https://doi.org/10.1080/19443994.2016.1155173.

Jiang, D.B., Jing, C., Yuan, Y., Feng, L., Liu, X., Dong, F., Dong, B., Zhang, Y.X., 2019. 2D–2D growth of NiFe LDH nanoflakes on montmorillonite for cationic and anionic dye adsorption performance. J. Colloid Interface Sci. 540, 398–409. https://doi.org/10.1016/j.jcis.2019.01.022.

Johnston, A.L., Lester, E., Williams, O., Gomes, R.L., 2021. Understanding Layered Double Hydroxide properties as sorbent materials for removing organic pollutants from environmental waters. Environ. Chem. Eng. 9, 13. https://doi.org/10.1016/j.jece.2021.105197.

Kareem, S.L., Mohammed, A.A., 2020. Removal of tetracycline from wastewater using circulating fluidized bed. Iraqi J. Chem. Pet. Eng. 21, 29–37. https://doi.org/10.31699/ijcpe.2020.3.4.

Khitous, M., Salem, Z., Halliche, D., 2015. Removal of phosphate from industrial wastewater using uncalcined MgAl-NO 3 layered double hydroxide : batch study and modeling Removal of phosphate from industrial wastewater using uncalcined MgAl-NO 3 layered double hydroxide : batch study and modeling. Desalin. Water Treat. https://doi.org/10.1080/19443994.2015.1077745.

Kostic, M., Radovi, M., Velinov, N., Najdanovi, S., Boji, D., Hurt, A., Boji, A., 2018. Synthesis of mesoporous triple-metal nanosorbent from layered double hydroxide as an e ffi cient new sorbent for removal of dye from water and wastewater. Ecotoxicol. Environ. Saf. 159, 332–341. https://doi.org/10.1016/j.ecoenv.2018.05.015.

Kute, M., Deo, H., Pai, S., 2018. Adsorption of methylene blue using Ni / Fe layered double hydroxide. Pharma Innov. J. 7, 190–192.

Lei, C., Pi, M., Kuang, P., Guo, Y., Zhang, F., 2017. Organic dye removal from aqueous solutions by hierarchical calcined Ni-Fe layered double hydroxide: isotherm, kinetic and mechanism studies. J. Colloid Interface Sci. 496, 158–166. https://doi.org/10.1016/j.jcis.2017.02.025.

Li, Y., Bi, H., Shi, X., 2015. Simultaneous adsorption of heavy metal and organic pollutant onto citrate-modified layered double hydroxides with Dodecylbenzenesulfonate 1, *. Environ. Eng. Sci. 32, 666–675. https://doi.org/10.1089/ees.2014.0489.

Li, Y., Bi, H.Y., Liang, Y.Q., Mao, X.M., Li, H., 2021. Synthesis of novel magnetic rhamnolipid-activated layered double hydroxides nanocomposite for simultaneous adsorption of Cu(II) and m-cresol from aqueous solution. Powder Technol. 386, 350–360. https://doi.org/10.1016/j.powtec.2021.03.048.

Lu, Y., Jiang, B., Fang, L., Ling, F., Gao, J., Wu, F., Zhang, X., 2016. High performance NiFe layered double hydroxide for methyl orange dye and Cr(VI) adsorption. Chemosphere 152, 415–422. https://doi.org/10.1016/j.chemosphere.2016.03.015.

Lyu, F., Yu, H., Hou, T., Yan, L., Zhang, X., Du, B., 2018. Efficient and fast removal of Pb2+ and Cd2+ from an aqueous solution using a chitosan/Mg-Al-layered double hydroxide nanocomposite. Colloid Interface Sci. https://doi.org/10.1016/j.jcis.2018.12.049.

Ma, S., Chen, Q., Li, H., Wang, P., Islam, S.M., Gu, Q., Yang, X., Kanatzidis, M.G., 2014. Highly selective and efficient heavy metal capture with polysulfide intercalated layered double hydroxides. J. Mater. Chem. A 2, 10280–10289. https://doi.org/10.1039/c4ta01203h.

Madejova, J., 2003. FTIR techniques in clay mineral studies. Vib. Spectrosc. 31, 1–10. https://doi.org/10.1016/S0924-2031(02)00065-6.

Mallakpour, S., Naghdi, M., 2020. Design and identification of poly (vinyl chloride)/layered double hydroxide@MnO2 nanocomposite films and evaluation of the methyl orange uptake: linear and non-linear isotherm and kinetic adsorption models. New J. Chem. 44, 6510–6523. https://doi.org/10.1039/d0nj01162b.

Mishra, A.K., Allauddin, S., Narayan, R., Aminabhavi, T.M., Raju, K.V.S.N., 2012. Characterization of surface-modified montmorillonite nanocomposites. Ceram. Int. 38, 929–934. https://doi.org/10.1016/j.ceramint.2011.08.012.

Mittal, J., 2021. Recent progress in the synthesis of layered double hydroxides and their application for the adsorptive removal of dyes: a review. Environ. Manage. 295,. https://doi.org/10.1016/j.jenvman.2021.113017 113017.

Mohammed, A.A., 2015. Biosorption of lead, cadmium, and zinc onto sunflower shell : equilibrium, kinetic, and thermodynamic studies. Iraqi J. Chem. Pet. Eng. 16 (16), 91–105.

Mohammed, A.A., Brouers, F., Isra'a Sadi, S., Al-Musawi, T.J., 2018. Role of Fe3O4 magnetite nanoparticles used to coat bentonite in zinc(II) ions sequestration, Environmental Nanotechnology, Monitoring and Management. Environmental Nanotechnology, Monitoring & Management. https://doi.org/10.1016/j.enmm.2018.04.004.

Mohammed, A.A., Kareem, S.L., 2019. Adsorption of tetracycline fom wastewater by using Pistachio shell coated with ZnO nanoparticles : equilibrium, kinetic and isotherm studies. Alexandria Eng. J. 58, 917–928. https://doi.org/10.1016/j.aej.2019.08.006.

Mohammed, A.A., Kareem, S.L., 2021. Enhancement of ciprofloxacin antibiotic removal from aqueous solution using zno nanoparticles coated on pistachio shell. Desalin. Water Treat. 213, 229–239. https://doi.org/10.5004/dwt.2021.26674.

Mohammed, A.A., Al-Musawi, T.J., Kareem, S.L., Zarrabi, M., Al-Ma'abreh, A.M., 2020. Simultaneous adsorption of tetracycline, amoxicillin, and ciprofloxacin by pistachio shell powder coated with zinc oxide nanoparticles. Arab. J. Chem. 13, 4629–4643. https://doi.org/10.1016/j.arabjc.2019.10.010

Mortaheb, H.R., Kosuge, H., Mokhtarani, B., Amini, M.H., Banihashemi, H.R., 2009. Study on removal of cadmium from wastewater by emulsion liquid membrane. Hazard. Mater. 165, 630–636. https://doi.org/10.1016/j.jhazmat.2008.10.039.

Mu'azu, N.D., Jarrah, N., Kazeem, T.S., Zubair, M., Al-Harthi, M., 2018. Bentonite-layered double hydroxide composite for enhanced aqueous adsorption of Eriochrome Black T. Appl. Clay Sci. 161, 23–34. https://doi.org/10.1016/j.clay.2018.04.009

Najwa, M., Mohamed, N., Bukhari, F., Suah, M., 2020. Electrochemical removal of cadmium from a sulphate solution using a three-dimensional electrode. Alexandria Eng. J. 1–9. https://doi.org/10.1016/j.aej.2020.07.027.

Nava-Andrade, K., Carbajal-Arízaga, G.G., Obregón, S., Rodríguez-Gonźalez c, V., 2021. Layered double hydroxides and related hybrid materials for removal of pharmaceutical pollutants from water. Environ. Manage. 288

Nguyen, D.T.C., Le, H.T.N., Nguyen, T.T., Nguyen, T.T.T., Liew, R. K., Bach, L.G., Nguyen, T.D., Vo, D.V.N., Tran, T.V., 2021. Engineering conversion of Asteraceae plants into biochars for exploring potential applications: a review. Sci. Total Environ. 797,. https://doi.org/10.1016/j.scitotenv.2021.149195 149195.

Peighambardoust, S.J., Pourabbas, B., 2007. Preparation and characterization of nylon-6/PPy/MMT composite of nanocomposite. J. Appl. Polym. Sci. 106, 697–705. https://doi.org/10.1002/app.

Peighambardoust, S.J., Foroutan, R., Peighambardoust, S.H., Khatooni, H., Ramavandi, B., 2021. Decoration of Citrus limon wood carbon with Fe3O4 to enhanced Cd2+ removal: a reclaimable and magnetic nanocomposite. Chemosphere 282,. https://doi.org/10.1016/j.chemosphere.2021.131088 131088.

Prasad, C., Tang, H., Liu, W., 2018. Magnetic Fe3O4 based layered double hydroxides (LDHs) nanocomposites (Fe3O4/LDHs): recent review of progress in synthesis, properties and applications. J. Nanostruct. Chem. 8, 393–412. https://doi.org/10.1007/s40097-018-0289-y.

Puzyrnaya, L.N., Pshinko, G.N., Zub, V.Y., Zuy, O.V., 2020. Removal of Cu(II), Co(II) and Cd(II) from water solutions by layered-double hydroxides with different [Mg(II)]/[Fe(III)] molar ratios. Bull. Mater. Sci. 43. https://doi.org/10.1007/s12034-019-1969-z.

Rathee, G., Singh, N., Chandra, R., 2020. Simultaneous elimination of dyes and antibiotic with a hydrothermally generated NiAlTi layered double hydroxide adsorbent. ACS Omega 5, 2368–2377. https://doi.org/10.1021/acsomega.9b03785.

Sahu, S., Kar, P., Bishoyi, N., Mallik, L., Patel, R.K., 2019. Synthesis of polypyrrole-modified layered double hydroxides for efficient removal of Cr(VI). J. Chem. Eng. Data 64, 4357–4368. https://doi.org/10.1021/acs.jced.9b00444.

Santamaría, L., Devred, F., Gaigneaux, E.M., Vicente, M.A., Korili, S.A., Gil, A., 2020. Effect of the surface properties of Me2+/Al layered double hydroxides synthesized from aluminum saline slag wastes on the adsorption removal of drugs. Micropor. Mesopor. Mater. 309,. https://doi.org/10.1016/j.micromeso.2020.110560 110560.

Santos, R.M.M. dos, Gonçalves, R.G.L., Constantino, V.R.L., Santilli, C.V., Borges, P.D., Tronto, J., Pinto, F.G., 2017. Adsorption of Acid Yellow 42 dye on calcined layered double hydroxide: Effect of time, concentration, pH and temperature. Appl. Clay Sci. 140, 132–139. https://doi.org/10.1016/j.clay.2017.02.005.

Seddighi, H., Khodadadi Darban, A., Khanchi, A., Fasihi, J., Koleini, J., 2017. LDH(Mg/Al:2)@montmorillonite nanocomposite as a novel anion-exchanger to adsorb uranyl ion from carbonate-containing solutions. J. Radioanal. Nucl. Chem. 314, 415–427. https://doi.org/10.1007/s10967-017-5387-7.

Shahid, M., Farooqi, Z.H., Farooq, R.B., Arif, M., Azam, M., Umar, A.I., 2021. Multi-functional organic–inorganic hydrogel microspheres as efficient catalytic system for reduction of toxic dyes in aqueous medium. De Gruyter 236, 87–105. https://doi.org/10.1515/zpch-2020-1739.

Shan, R., Yan, L., Yang, K., Yu, S., Hao, Y., 2014. Magnetic Fe3O4/MgAl-LDH composite for effective removal of three red dyes from aqueous solution. Chem. Eng. 252, 38–46. https://doi.org/10.1016/j.cej.2014.04.105.

Shan, R. ran, Yan, L. guo, Yang, K., Hao, Y. feng, Du, B., 2015. Adsorption of Cd(II) by Mg-Al-CO3- and magnetic Fe3O4/Mg-Al-CO3-layered double hydroxides: Kinetic, isothermal, thermodynamic and mechanistic studies. Hazard. Mater. 299, 42–49. https://doi.org/10.1016/j.jhazmat.2015.06.003

Shattar, S.F.A., Zakaria, N.A., Foo, K.Y., 2017. Utilization of montmorillonite as a refining solution for the treatment of ametryn, a second generation of pesticide. J. Environ. Chem. Eng. 5, 3235–3242. https://doi.org/10.1016/j.jece.2017.06.031.

Shen, J., Duvnjak, Z., 2005. Adsorption kinetics of cupric and cadmium ions on corncob particles. Process Biochem. 40, 3446–3454. https://doi.org/10.1016/j.procbio.2005.02.016.

Shen, Y., Zhao, X., Zhang, X., Li, S., Liu, D., Fan, L., 2016. Removal of Pb2+ from the aqueous solution by tartrate intercalated layered double hydroxides. Korean J. Chem. Eng. 33, 159–169. https://doi.org/10.1007/s11814-015-0110-2.

Shin, H.S., Kim, J.H., 2016. Isotherm, kinetic and thermodynamic characteristics of adsorption of paclitaxel onto Diaion HP-20. Process Biochem. 51, 917–924. https://doi.org/10.1016/j.procbio.2016.03.013.

Tan, Y., Yin, X., Wang, C., Sun, H., Ma, A., Zhang, G., Wang, N., 2019. Sorption of cadmium onto Mg-Fe Layered Double Hydroxide (LDH)-Kiwi branch biochar. Environ. Pollut. Bioavailab. 31, 189–197. https://doi.org/10.1080/26395940.2019.1604165.

Tran, H.N., Lin, C., Han, S., Chao, H., 2018. Efficient removal of copper and lead by Mg / Al layered double hydroxides intercalated with organic acid anions : adsorption kinetics, isotherms, and thermodynamics. Appl. Clay Sci. 154, 17–27. https://doi.org/10.1016/j.clay.2017.12.033.

Vijayaraghavan, K., Yun, Y., 2008. Bacterial biosorbents and biosorption. Biotechnol. Adv. 26, 266–291. https://doi.org/10.1016/j.biotechadv.2008.02.002.

Vulić, T.J., Bošković, G.C., 2010. Mg-Cu-Al layered double hydroxides based catalysts for the reduction of nitrates in aqueous solutions. Acta Period. Technol. 41, 131–139. https://doi.org/10.2298/APT1041131V.

Wang, Z., Fang, D.M., Li, Q., Zhang, L.X., Qian, R., Zhu, Y., Qu, H.Y., Du, Y.P., 2012. Modified mesoporous silica materials for on-line separation and preconcentration of hexavalent chromium using a microcolumn coupled with flame atomic absorption spectrometry. Anal. Chim. Acta 725, 81–86. https://doi.org/10.1016/j.aca.2012.03.005.

Wang, J., Wang, P., Wang, H., Dong, J., Chen, W., Wang, X., Wang, S., Hayat, T., Alsaedi, A., Wang, X., 2017. Preparation of molybdenum disulfide coated Mg/Al layered double hydroxide composites for efficient removal of chromium(VI). ACS Sustain. Chem. Eng. 5, 7165–7174. https://doi.org/10.1021/acssuschemeng.7b01347.

Wong, C., Barford, J.P., Chen, G., Mckay, G., 2013. Kinetics and equilibrium studies for the removal of cadmium ions by ion exchange resin. Environ. Chem. Eng. 2, 698–707. https://doi.org/10.1016/j.jece.2013.11.010.

Yang, Z., Ji, S., Gao, W., Zhang, C., Ren, L., Tjiu, W.W., Zhang, Z., Pan, J., Liu, T., 2013. Magnetic nanomaterial derived from graphene oxide/layered double hydroxide hybrid for efficient removal of methyl orange from aqueous solution. J. Colloid Interface Sci. 408, 25–32. https://doi.org/10.1016/j.jcis.2013.07.011.

Yang, S., Wang, L., Zhang, X., Yang, W., Song, G., 2015. Enhanced adsorption of Congo red dye by functionalized carbon nanotube/mixed metal oxides nanocomposites derived from layered double hydroxide precursor. Chem. Eng. 275, 315–321. https://doi.org/10.1016/j.cej.2015.04.049.

Yu, J., Zhu, Z., Zhang, H., Qiu, Y., Yin, D., 2018. Mg–Fe layered double hydroxide assembled on biochar derived from rice husk ash: facile synthesis and application in efficient removal of heavy metals. Environ. Sci. Pollut. Res. 25, 24293–24304. https://doi.org/10.1007/s11356-018-2500-6.

Yuan, X., Wang, Y., Wang, J., Zhou, C., Tang, Q., Rao, X., 2013. Calcined graphene/MgAl-layered double hydroxides for enhanced Cr (VI) removal. Chem. Eng. 221, 204–213. https://doi.org/10.1016/j.cej.2013.01.090.

Zhang, X., Yan, L., Li, J., Yu, H., 2020. Adsorption of heavy metals by L-cysteine intercalated layered double hydroxide: Kinetic, isothermal and mechanistic studies. Colloid Interface Sci. 562, 149–158. https://doi.org/10.1016/j.jcis.2019.12.028.

Zhou, H., Jiang, Z., Wei, S., 2018. Adsorption of Cd (II) from Aqueous Solutions by a Novel Layered Double Hydroxide FeMnMg-LDH. Water Air Soil Pollut 229. https://doi.org/doi.org/10.1007/s11270-017-3597-9 Adsorption.

Zubair, M., Daud, M., McKay, G., Shehzad, F., Al-Harthi, M.A., 2017. Recent progress in layered double hydroxides (LDH)-containing hybrids as adsorbents for water remediation. Appl. Clay Sci. 143, 279–292. https://doi.org/10.1016/j.clay.2017.04.002.

Zubair, M., Jarrah, N., Khalid, A., Saood, M., 2018. Starch-NiFe-layered double hydroxide composites : Efficient removal of methyl orange from aqueous phase. Mol. Liq. 249, 254–264. https://doi.org/10.1016/j.molliq.2017.11.022.